TALLINN UNIVERSITY OF TECHNOLOGY
School of Information Technologies

Stephen Kabali IVEM 165524

TTÜ100 SATELLITE OPTICAL COMMUNICATION EXPERIMENT

Master's Thesis

Supervisor: Andres Eek

Tallinn 2018

TALLINNA TEHNIKAÜLIKOOL
Infotehnoloogia teaduskond

Stephen Kabali IVEM 165524

TTÜ100 SATELLIIDI OPTILISE KOMMUNIKATSIOONI EKSPERIMENT

Magistritöö

Juhendaja: Andres Eek

Tallinn 2018

Author’s declaration of originality

I hereby certify that I am the sole author of this thesis. All the used materials, references to the literature and the work of others have been referred to. This thesis has not been presented for examination anywhere else.

Author: Stephen Kabali

22.05.2019

Abstract

Different pieces of hardware like a microcontroller unit, infrared-transmitters and receivers, resistors, diode, LEDs, navigation and positioning units and possibly solar panels for power will be coupled together and programmed to create one unified complex product the, TTÜ100 satellite.

Aboard the TTÜ100 will be a series of communication modules both optical and RF based. The thesis is concentrating on designing a receiver for the optical communication module which will use lasers as carriers within both visible and invisible spectrums range.

Optical communication has gained vital importance over the years due to its unique properties such as broad bandwidth, license-free spectrum, high data rate, narrow bandwidth, small focusing area, easy and quick to deploy, less power consumption and small size compared to gain Rf antennas. Different communication systems using optical carriers in the near infrared spectrum to establish either terrestrial links within the Earth's atmosphere or inter-satellite/deep space links or ground-to-satellite/satellite-to-ground links have been created [1], [2].

The thesis has a total of five chapters. Chapter 1 covers the introduction part a brief history laser communication, RF (radio frequency) and optical communication comparison. Chapter 2 will more extensively cover FSO systems, design factors, and channel modeling. Chapter 3 is dedicated to a crucial part of the research which is optical sensors. Designing the receiver module and what to look out for when doing component selection will be covered in chapter 4. Finally, a conclusion and future works will be in the last chapter 5.

This thesis is written in English and is 49 pages long, including 5 chapters, 28 figures, and 10 tables.

Annotatsioon

TTÜ100 satelliidi optilise kommunikatsiooni eksperiment

TTÜ100 satelliidi projekt hõlmab enda all erinevaid riistvara komponente ning tarkvara lahendusi. Riistvara komponentide alla kuuluvad näiteks mikrokontrollerid, infrapuna LED-id, takistid, dioodid, positsioneerimise seadmed, päikesepaneelid jne.

TTÜ100 satelliidi pardal kasutatakse optilisi ja raadiosageduslikke kommunikatsiooni mooduleid. Antud lõputöö keskendub optilisele kommunikatsiooni moodulile. Lähemalt uuritakse antud lõputöö käigus tundlikke optilise kiirguse vastuvõtjaid ja võimendeid infrapuna ja nähtava valguse laserite kiirguse vastuvõtuks.

Optiline kommunikatsioon on viimastel aastatel saanud palju tähelepanu, kuna võimaldab suurt ribalaiust, litsentsivaba spektrit, kõrget sidekiirust, lihtsat ja kiiret seadistust, väikest voolutarvet ning väikest kaalu. Erinevad sidesüsteemid kasutavad optilist sidet lähi-infrapuna spektris maapealse side loomiseks, satelliitide vahelise side, süvakosmose side või satelliidilt-maale/maalt-satelliidile side jaoks[1], [2].

Antud lõputöö koosneb viiest peatükist. Peatükk 1 antakse ülevaade laser kommunikatsiooni ajaloost, ühtlasi võrreldakse raadiosagedusliku ja optilise erinevusi. Peatükk 2 kirjeldab kuidas disainida ja modelleerida sidekanaleid vaba ruumi optilise side (FSO) süsteemide jaoks. Peatükk 3 keskendub optilistele sensoritele, mis on antud lõputöö tuumaks. Vastuvõtja mooduli disainimine ning komponentide valiku põhjendused on kirjeldatud peatükis 4. Kokkuvõtte ning edasine vajalik uurimistöö on esitletud peatükis 5.

Lõputöö on kirjutatud inglise keeles ning sisaldab teksti 49 leheküljel, 5 peatükki, 28 joonist, 10 tabelit.

List of abbreviations and terms

DPI	*Dots per inch*
TTU	Tallinn University of Technology
ESA	European Space Agency
NASA	National Aeronautics and Space Administration
CNES	Centre for Space Studies
OBC	Onboard Computer
UAV	Unmanned Aerial Vehicle
ADC	Analog to Digital Converter
DAC	Digital to Analogue Converter
FSO	Free-Space Optical Communication
IrDA	Infrared Data Association
IrLD	Infrared Laser Diode
IR	Infrared
VASI	visual approach slope indicator
RF	Radio Frequency
APD	Avalanche photodiode
QoS	Quality of service
OWSN	Optical wireless network
GEO	Geostationary earth orbit
LEO	Low earth orbit
LOS	Line of sight
OWTN	Optical wireless terrestrial network
OWHN	Optical wireless home network
ISL	Inter-satellite link
LTE	Long-term evolution
RFID	Radio frequency identification
GaAs	Gallium arsenide
InGaAs	Indium gallium arsenide
ACF	Advanced Coma-free
UHTC	Ultra-High Transmission Coatings

Table of contents

List of figures

List of tables

1 Introduction

1.1 State of the Art Overview

Research in the field of free space optical (FSO) communication is a hot topic. As recent as April 2019, NASA awarded pathfinder digital a contract to study the feasibility of developing a portable test and research platform to aid in FSO satellite networks' system design.[3] This study should be mainly focused on studying hybrid laser communication/ RF systems, ground stations and their ability to efficiently communicate with in-space optical terminals, development of space-related problem mitigation techniques, etc.

A team of researchers from different universities such as Oxford, Munster, and Exeter built a working all optical neural network on a single chip with no optical to electronic conversions [4]. More research is ongoing in the field of multi-photon quantum states on silicon[4]–[7], free space-based quantum key distribution and systems to handle information at a quantum level.[8] A global market study also shows that there will be growing demand for FSO systems between 2019 to 2025 in different markets such as defense, healthcare, data transmission, last Mile access, space applications, etc[9].

Why laser communication? From basic telecommunications, needs to have a large parabolic mirror to focus the beam, laser communication, however, doesn't function on this principle. A laser communication system operating at 1 Gb/s requires an aperture of approximately 30 cm. In contrast, a 1 Gb/s millimeter wave (RF) system needs a significantly more substantial aperture, 2-2.75m, the shorter wavelength in optical communication offers better beam focusing. Since the invention of lasers in 1960, they have been considered for space communication.[10] With their capability for the transfer of data at extremely high rates, it was soon realized that, advancements in component performance and systems engineering needed to be made, particularly for space deep space communication.[11]

Advancements in system requirements, design, data formatting, and component architecture over the past thirty years have not only made laser communications an

attractive approach to space-earth link applications but also opened up new fields of research.

1.2 Thesis task specification

A total of four dual (both visible and invisible) wavelengths infrared laser diodes (IrLEDs) rated 0.2 Watts each were embedded within the TTÜ100 satellite that will be launched 500km in the low earth orbit. The task is to design a receiver capable of receiving data up to 10 kbps from the satellite. For the data transfer, this system is using on-off keying (OOK).

1.3 The future of laser communication

Free space optical networks (FSO) systems have enormous potential for high capacity of over Gbps per link. The transmission is typically conducted using a line of sight (LOS) propagation with a narrow directional beam over a long distance. FSO channels are deployable on a wide range of areas from home to terrestrial, and to the satellite. Those unique properties have sparked a significant amount of research. However, research on fully harvesting the potential of FSO networks is still in its infant stage, and many notable and challenging problems still need to be solved.

There are plans in the future to test laser communications in deep space on the Psyche mission to the main-belt asteroid 16 Psyche, planned to launch in 2022 [11]. The system is called Deep Space Optical Communications,[12] and is expected to boost spacecraft communications performance and efficiency exponentially over conventional means.

Just like the projects mentioned above, the TTÜ100 is not that much different; experimental laser communication technology will be used to establish a one-way link from the TTÜ100 satellite to a receiver on earth. The anticipated data will consist of data about the status of the onboard systems that is, an onboard computer (OBC), batteries, cameras, sensors, solar panels and many more.

1.4 Commercial usage of Laser communication

Multinational corporations like Golbriak space, SpaceX, Facebook and Google and a series of start-ups are currently pursuing various concepts with laser communication technology at the core of their innovations. The most promising commercial applications can be found in the interconnection of satellites or high-altitude platforms to build up high-performance optical backbone networks. Other applications include the transmission of large data amounts directly from a satellite, aircraft or (UAV) to the ground [13]–[15]

1.5 Advantages of Laser over conventional RF

1.5.1 RF Communication

For more than a century, RF technology has and is still being used for communication. It relays on the propagation of wireless electromagnetic signals for data communication. In 1901 Marconi [16], [17] achieved his first successful data transmission using the RF signal from one remote station to other. Initially, the band of RF is based on the very low frequency of kilo Hertz to MHz range. It can extend to the different frequency range for microwave communication. At the initial phase, radio frequency communication was just limited to the lower frequency band for the data transmission and used for radio and some military applications. But as time went by, the frequency range extended and increased into hundreds of gigahertz due to the need for higher data rate and noise immunity in the field. Various coding techniques are used to make data secure and for transmission efficiency [18].

Over the years, it had been believed that only two types of the electromagnetic spectrum could be used for communication in the Earth's atmosphere. Those being; visible light, and the other being a radio with only frequencies between about 30 MHz and 30 GHz viable for space communication. Table 1 below show more about the frequencies according to the international telecommunication union (ITU). Recent studies, however, have shown that the invisible spectrum can also be tapped for free space communication [19].

Table 1. below shows ITU Radio bands, frequencies, and wavelengths.

Band Number	Abbreviation	Frequency range	Wavelength range†
4	VLF	3 kHz to 30 kHz	10 km to 100 km
5	LF	30 kHz to 300 kHz	1 km to 10 km
6	MF	300 kHz to 3000 kHz	100 m to 1000 m
7	HF	3 MHz to 30 MHz	10 m to 100 m
8	VHF	30 MHz to 300 MHz	1 m to 10 m
9	UHF	300 MHz to 3000 MHz	10 cm to 100 cm
10	SHF	3 GHz to 30 GHz	1 cm to 10 cm
11	EHF	30 GHz to 300 GHz	1 mm to 10 mm
12	THF	300 GHz to 3000 GHz	0.1 mm to 1 mm

1.5.2 Optical Communication

Communication at a distance using light as a medium of information transfer is called optical communication. Optical communication can be as simple as Morse code or as complex as inter-satellite communication or satellite to earth communication with the use of sophisticated electronics. One of the first documented cases of optical communication is date back in 1880 when Alexander Graham Bell and his assistant Charles Sumner Tainter invented the photophone [20]. There are however cases such as in 1867 when Philip Colomb of the British royal navy put into practice the use of flashing dots and dashes (modern-day Morse code) [21].

The earliest forms of optical communication included smoke signals, beacon fires, ship flags and so on. In the present day, flares are still used as distress signals in emergencies especially in sea vessels, or in places such as mountains and readily inaccessible areas. Ships captains and sailors watch out for lighthouses and pilots still follow lights on runways to position the planes accurately while landing.

Free-space optical (FSO) communication has been deployed in space, while terrestrial forms are naturally limited by geography, weather and the availability of light. Different types of optical transmission will be listed below.

The heliograph is probably one of the oldest methods of performing optical communication; its principle of operation involves a mirror to reflect sunlight to a distant observer. The person transmitting the signal tilts the mirror to reflect sunlight, the observer sees flashes of light and deciphers them to interpret the transmitted prearranged signaling code. Naval ships often use signal lamps and Morse code similarly.

To see the runway, aircraft pilots often use the visual approach slope indicator (VASI) projected light systems to land safely, especially at night. Military aircraft landing on an

aircraft carrier uses a similar method to land correctly on a carrier deck. The colored light system communicates the aircraft's height relative to a standard landing glideslope. In situations where the aircraft radios have failed, airport control towers still use Aldis lamps to transmit instructions to the pilots. Nowadays, several electronic systems rely on optical communication to transmit and receive information carried by pulses of light at super high speeds. Fiber-optic communication cables are now used to send the vast majority of the electronic data and long-distance telephone calls that are not conveyed by either radio, terrestrial microwave or satellite. Free-space optical communications are also used every day in various applications.

2 Free Space Optical Communication

2.1 Understanding FSO

Free Space Optical (FSO) systems, specifically, remote optical systems, are wireless media transmission frameworks that make utilization of free space as a transmission medium to convey visual information signals at high data rates. FSO exploration began in the 60s. National Aeronautics and Space Administration (NASA)'s Deep Space Optical Communications project is aimed at creating critical advancements for the usage of a deep space optical transceivers, and ground collector that will empower more than 10 times the information rate of a cutting-edge deep space RF framework (Ka-band) for comparable rocket mass and power[22][23][24]. The European Space Agency (ESA) began financing different FSO ventures since the mid of 1977, meaning to grow high-information rate laser interfaces in space. Albeit optical wireless connections give high information rates, FSO interchanges have not won so far despite a long investigative history. As new advances are made in optics and specialized gadgets, there has been a recharged, expanding enthusiasm for examining and improving wireless optical connections and receiving FSO innovation for wireless access systems. As of late, fruitful test [25] shown the practicality of FSO communication. Specialists at the German Aerospace Centre exhibited FSO information transmissions at 1.72 terabits per second over a range of 10.45 km [22], [26]. The FSO system could turn into a reasonable possibility for use in broadband wireless systems of the future generation networks. Wireless communications have gainful properties not found in wired connections, for example, the lower implementation cost because of the absence of ditching and running cables over 10s of kilometers, the simplicity of development of system topology, adaptable upkeep of working systems, et cetera. Wireless networks likewise enable clients of mobile gadgets to get to Internet connectivity whenever and in numerous areas. For example, IEEE 802.11 (Wi-Fi), Bluetooth, and IrDA are designed for short-distance wireless information transfers [23], as Long-Term Evolution (LTE) is intended for long-distance wireless communication for both mobile devices and data stations [22], [28]. To this point, FSO systems are thought to be a reliable supplementary alternative. Their plus points over radio wireless systems are noted below. Definite correlations between radio and optical wireless communication are found in [22], [29]–[31][32].

- Optical wireless connections give high information rates to help broadband information services. Commercial systems that support Gbps information rates are in existence.[22].

- FSO communication requires no license hence no compelling reason to get consent to utilize the optical channels; a lot of resources can be put to other works or saved for maintenance compared with different wireless RF-based technologies [22].

- Compared to RF systems, FSO networks are more immune to electromagnetic disturbances.

- Optical wireless communication systems are cheaper than RF systems regarding power consumption and component prices, [22].

- Because of narrow beam width and point-to-point transmission properties, unique optical connections have the attractive LPI/LPD (Low Probability of Intercept/Low Probability of Detection) features.

- Luminous sources with similar description can be reused in covering different regions or rooms in the working since light rays can't infiltrate opaque objects, bringing about small common obstruction [22].

2.2 Types of FSO Networks

Because of their high potential for a wide range of uses, FSO systems have been researched and utilized for systems that traverse a range from a couple of meters to more than a 1000s of kilometers. As outlined in Figure1, FSO systems can be ordered into three classes[22]:

1. Optical Wireless Satellite Networks (OWSNs)

2. Optical Wireless Terrestrial Networks (OWTNs)

3. Optical Wireless Home Networks (OWHNs)

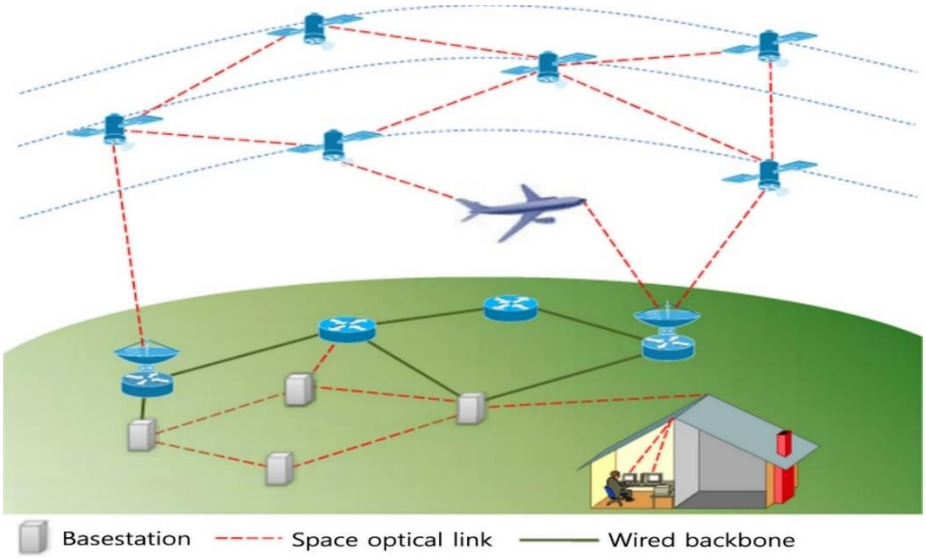

Figure 1. A conceptual topology of integrated optical wireless satellite, terrestrial, and home networks.

Based on the placement of optical transmitters and receivers and network distance [22]. It might be difficult to precisely outline these systems since different FSO sub-networks are merged and managed in general, as appeared in Figure. 1. Each class of the FSO system is reviewed in detail in this segment, and their attributes are abridged in Table 2[22]

Table 2. below show the characteristics of various wireless optical networks.

	OWSNs	OWTNs	OWHNs (IrDA)	OWHNs (MSD, White LED)
Location	Orbit	High/open place	Indoor	Indoor
Link distance	~84,000 km	~10 km	~ a few meters	~10s of meters
Channel	Vacuum channel	Air turbulent channel	Weak turbulent channel	Weak turbulent channel
RX/RX FOV	Very narrow	Narrow	30 degrees	Wide
Performance Limiting factors	Misalignment with long distance	atmospheric turbulence	Limited power for eye and LOS blockage safety	Limited power for eye safety a multi-path propagation
Hardware requirements	Precise PAT technology i.e., Automatic steerable gimbals/beams	Turbulence resistant design	Lightweight, portable and inexpensive components	Backbone between cells and MSD- holographic optical diffuser
Misc	Long distance coverage is hard to maintain	Various impairment factors	Short range point to point link	Exploiting reflection

2.3 Design Factors

Critical factors in designing networks are analyzed here. These factors influence the performance of FSO networks and point to the direction of required technology development, algorithms, and protocols.

2.3.1 FSO Channel categorization

FSO uses an unguided beam that propagates through free space as the transmission medium. Such a light, open space channel should be analyzed and characterized. The typical FSO channel conditions fluctuate and deteriorate due to atmospheric turbulence. Indeed, atmospheric turmoil has been one of the leading clogging factors of practical deployment. Atmospheric impairment and disturbance degrade FSO channel performance and makes it hard to achieve constant availability and reliability. It is shown

in [22], [33] that if a deep fade lasts for $\sim 1 - 100\mu s$ on the multiple Gbps optical channel, up to 10^{-9} consecutive bits might be lost. The refractive index structure parameter, typically denoted as C_n^2 , represents the strength of the atmospheric turbulence, which has a substantial impact on channel fading [22], [34], [35][36]. There are many atmospheric turbulence factors such as weather phenomena and scintillation by pressure, humidity, and temperature that affect FSO link quality. When weather conditions are severe, the performance of a free space link will be significantly hampered. However, it is found that channel availability can be achieved with high probability even under severe weather conditions. According to [22], [37], atmospheric attenuation is continuously low, over 99% as measured in three major U.K. cities. When a sufficient power budget is applied, an FSO link availability of up to 99.5% is achievable. Scintillation, the temporary spatial variation of light intensity, degrades the performance of FSO links even in clear weather. In particular, the changes in temperature dominate the refractive index structure parameter. According to sources [22], [35], the scintillation effects induced by pressure and humidity are relatively small, but the results of temperature are more significant to link quality. The low channel quality problem usually occurs in satellite-to terrestrial and inter-terrestrial connections, since air turbulence mostly causes them. To further understand channel conditions, various statistical channel models were proposed in the literature, such as log-normal, K-, lognormal-Rician, and Gamma-Gamma distributions [22], [38]. However, the inter-satellite links and OWHNs are usually free from atmospheric influences since the inter-satellite optical beams propagate through the vacuum of space and the distance of OWHN links is negligibly short.

2.3.2 Link reliability

The availability and reliability of wireless optical links are essential factors for FSO networks. If the wireless optical links suffer from low availability and reliability, the transmissions will be interrupted, and the overall performance of the FSO network will be degraded. Several sources deteriorate FSO link quality. In OWTNs, atmospheric turbulence is the main cause of link performance degradation. The narrow beam property of an FSO link is another cause of weak link connectivity. A typical optical beam propagates with a narrow divergence of a few mRads, and the Field of View (FOV) at the receiver is also small [22], [39], [40]. Due to these small angles, link loss or inaccurate alignment happens. Thus, Precise pointing, Acquisition, and Tracking (PAT) techniques are indispensable. In the case of mobile platforms such as satellites and airplanes, PAT

techniques become more challenging. Also, optical beams cannot penetrate non-transparent bodies, so if there is any stationary obstacle on the LOS path between two FSO transceivers, it would be impossible to form a link. Even though a wireless optical link exists, it suffers from temporary outages caused by moving objects like birds or snow. A straightforward approach achieves high availability and reliability by placing FSO devices where there is less probability of disturbance by objects and where the weather conditions are better on average. However, there are still opportunities to achieve higher availability and reliability of FSO links by considering and addressing one or more of the sources that affect them. Viable approaches to keep strengthening the availability and reliability of FSO channels have been proposed in the literature. These include autonomous PAT mechanisms [22], [40]–[42], diversity techniques [22], [43], [44], hybrid RF/FSO systems [22], [31], [45], among others.

2.3.3 Areas to automation for improved performance

There are trade-offs when operating FSO links between manually or by automation to establish/maintain link connections[22]. The degree of automatic operation depends on the specific application. If the FSO link is deployed in an area with high reliability and does not need to be changed in a direction for an extended period, it is possible to use manual operation with simple tracking mechanisms to save on costs. However, OWSNs, for example, require a high level of automation for topology control, since it is impossible to manipulate the direction once satellites have been launched. If FSO transceivers operate autonomously, self-configuration and self-healing algorithms should be developed and incorporated into the system [22], [42], [46].

2.3.4 Quality of service

The broadband serviceability of FSO networks is one of its promising advantages due to a very high-frequency band. FSO networks will surpass wireless radio networks in this capacity since FSO links pose no limitations on data rate [22], [47]. According to [22], [29], a 1.55 μm laser operating at a 200 THz frequency provides almost 200,000 times more capacity than a 2 GHz microwave link. The FSO links offer a competitive solution to the “last-mile” problem [22], [29], increasing the capacity of existing wireless networks [22], [48], and constituting an essential component for the next generation of broadband wireless communication networks. However, the capacity of FSO links is limited by transceiver performance [47] and eye safety constraints [27], even though data rates of

multiple Gbps can be achieved. How much capacity is made is determined by the aggregate of individual traffic flows passing through the FSO link. In addition to the broadband demand, various QoS requirements, such as end-to-end transmission delay, jitter, packet loss rate, and fairness, should be taken into consideration when designing networking algorithms and protocols in FSO networks. For example, the end-to-end delay is an important factor due to the long round trip distance in OWSNs [22], [36], while fairness may be a concern for an OWHN in a room serving multiple devices. The current congestion control mechanism in the Transmission Control Protocol (TCP) may not work well in an FSO network and could lead to reduced throughput performance, and thus more flexible protocols should be developed for FSO networks.

2.3.5 Safety concerns

High-power beams suppress atmospheric disturbance and make it possible to further meet the required data rates under severe weather conditions [22]. Although FSO transmissions usually do not cause mutual interference (unless pointing to each other), laser sources beyond a certain power threshold are harmful to the human body, in particular, the eyes. Thus, it is important to enforce a limitation on laser-emission power in optical wireless networks. Laser safety standards have been established, such as ANSI Z136.1 and IEC 60825-1 [22], [30]. According to IEC 60825-1, the objective is to protect the human body from excessive laser radiation ranging from 180 nm to 1 mm in wavelength [49], by classifying lasers and laser products based on their degree of hazard [22]. The optical beams in Class 1 and two are considered completely safe except when direct and lengthy exposure is involved. The Class 3 beams achieve a good power budget but are not recommended to come in contact with the human body. Interested readers are referred to [22], [30], [37] for detailed information. The safety regulations degrade the performance of FSO systems, i.e., the constraints on transmit power [30]. Operating low power sources requires the availability of highly sensitive receivers, which may suffer from more interference from the environment.

2.4 Channel modeling

It’s important to analyze a system and account for some parameters to aid in the construction of prototypes such as amplifiers, ADCs and so on. Through doing this, it’s possible to understand if the constructed system is feasible or not.

The model used doesn't consider the scattering coefficient, the field of view (FOV) and some other elements of this work due to lack of some components in the design such as the focusing optics on the transmitter. Should anyone or myself wish to continue with this work, or improve the design, these parameters and equations would be useful.

2.4.1 Scattering coefficient

In this context, scattering refers to the radiation of photons into different directions from the optical source through the transmission channel, in this case, space. There are actually three different types of scattering, namely: Mie scattering, Rayleigh scattering, and Geometrical scattering. The greater the distance between the transmitter and receiver, the greater the scattering. Should also note that different wavelengths in the light spectrum are affected differently. The smaller the wavelength, the more resistant it is to scatter. Scattering is denoted with equation 1 below[50].

$$scattering = \frac{3.91}{Range}\left(\frac{lmd}{550nm}\right)^{-q} \quad (1)$$

Where:

Range = visibility range in kilometers

lmd = transmission wavelength in nanometers

q = scattering particles distribution size

$$q = \begin{cases} 1.6 \; for \; Range > 50Km \\ 1.3 \; for \; 6Km < Range < 50Km \\ 0.585 Ramge^{1/3} for \; Range < 6Km \end{cases}$$

2.4.2 Received Power

Received power typically refers to the power at the transmitter after the signal navigates through the transport medium, in this case, being free space[51]–[53].

$$\Pr(W) = Pt * Gt * S * Gr \quad (2)$$

$$\Pr(dB) = Pt + Gt + S + Gr \quad (3)$$

where Pr is the received power which we can denote in either dB or Watts(W). The gain of transmitter $Gt = \left(\frac{16}{\theta a.\theta b}\right)$ where θa and b refer to the divergent angles of the transmitter used to create an elliptical representation of the signal on the ground.[51] When the area of the ellipse created is divided by the spherical area of the signal on the ground, we get

the value 16. In one angle systems, instead of θa and b, θ^2 can be used to achieve the same result. The gain of the receiver is denoted as $Gr = \left(\frac{\pi dr}{\lambda}\right)^2$ where dr receiver diameter and λ is the wavelength used. S in this case is the free space loss also represented as $20log10\left(\frac{\lambda}{4\pi R}\right)$ in the equation 3 and R refers to the link range[50], [51].

2.4.3 Signal to noise ratio (SNR)

To properly optimize any communication system, the signal to noise ratio is one of the import parameters that need to be found. It is measured in dB and denoted as:

$$SNR = \frac{Signal\ power}{\text{Noise power}} \quad (4)$$

2.4.4 Photon Energy

To properly optimize the system, it's necessary to know what the photon energy measured in joules (J). Knowing this will help in other calculations later. Photon energy is denoted in equation 5 below as:

$$E_{ph} = hc/\lambda \quad (5)$$

Where $h = 4.135 * 10^{-15} eV.sec$ Planck's constant and $c = 3 * 10^8 m/s$ the speed of light and λ which is wavelength.

2.4.5 Receiver FOV (Field of View)

In an FSO system, FOV is a very important parameter. Received power can be dependent on the FOV of the receiver. To calculate the FOV in this specific system, I will rely on two critical parameters. The receiver chip size and the focal length of the telescope used all denoted in the equation 6 below: A smaller FOV is good since it reduces the scattered light and the waveform received will be closer to the one at the transmitter.[53]

$$FOV = 2 * Tan^{-1}\left[\frac{Chip\ size}{focal\ length}\right] \quad (6)$$

2.4.6 Propagation loss

All communication systems are bound to have some losses, either during signal generation, transmission, path losses or even during the receiving of information. FSO systems just like any other systems are not immune to these losses. These losses are called

attenuation. Different factors can contribute to signal attenuation such as the distance of transmission (distance between transmitter and receiver), weather conditions, scattering, and many more other causes. In any communication system, attenuation is expected but measures are usually taken to ensure there is at least a signal received with a reasonable signal to noise ratio (SNR).

Now, to clearly calculate the attenuation, elements of Beer's law equation are used which states that, when a ray of monochromatic light goes through a medium, its intensity is bound to decrease exponentially as transmission range (R) increases due to medium absorption. It can be denoted in equation 7 below:

$$T(R) = -\frac{P(R)}{P(src)} \tag{7}$$

Where:

T(R): transmission at R

P(R): transmitted power at R

P(scr): transmitted power at the source

Now, using the logarithmic functions of equation 7 above, the scattering equation with Beer's equation to get the ultimate attenuation equation 8 below. Some factors that are not considered in the equation are listed in table 3 below.

$$T(R) = \log e^{\left(\left(\frac{3.91}{Visibility}\right)*\left(\frac{lmd(nm)}{550nm}\right)^{-q}*R\right)}\, dB \tag{8}$$

Table 3. Attenuation estimate ratings of different conditions.

Infrared spectrum	Attenuation in dB/km
Clear space/air	-1 to -5
Planes, birds…etc.	0 to -20
Light Mist	-1 to 25
Scintillation	0 to -3
Light rain	-1 to -10
Heavy rain	-25 to -40
Medium fog	-1 to -120
Thick fog	-1 to -300

The values listed in table 3 are dependent on the wavelength used. that's why clear space/air and thick fog and other factors begin at -1. Different wavelengths have different propagation properties in different mediums.

3 Optical Sensors/detectors

An optical sensor or detector is any photoreactive or photosensitive device that is capable of changing state either physically or internally. The state in most cases is an electric signal with Ohmic characteristics and of given frequency that is generated by a photoreactive surface when exposed to light. The electric signal can have a very small or relatively big signature depending on the light source and receiver amplification.

3.1 Types of Sensors

When it comes to optical or light detectors and receivers, there is a wide range of them depending on the wavelength and spectrum, some perform better than others because of the material used for construction, yet others are tuned to achieve maximum sensitivity at a given sensitivity. By optimizing optical detectors this way, it helps the user to have more control over some parameters such as the noise floor, responsiveness, and signal to noise ratio (SNR). The are many sensors out there that target specific wavelengths. The list below shows some of the existent types of receivers and their target spectrums.

- PIN diode sensors
- APD sensors
- Photomultiplier tubes
- Multi-Pixel Photon Counters (silicon photomultipliers)

some characteristics from different photodetector groups are shown in table 4 below. APD stands for avalanche photodiode, MPPC is multi-pixel photon counter and PMT is photomultiplier tube in context to table 4.

Table 4. Characteristics of photodetectors

characteristics	PIN	APD	MPPC	PMT
Gain	1	10^2	to 10^6	to 10^7
Sensitivity	Low	Medium	High	High
Operation voltage(V)	5	100 to 500	30 to 60	800 to 1000
Large area	No	No	Scalable	yes
Multi-channel with narrow gap	Yes	Yes	Yes	No
Readout circuit	Complex	Complex	Simple	Simple
Noise	Low	Middle	Middle	Low
Uniformity	Excellent	Good	Excellent	Good
Response time	Fast	Fast	Very Fast	Fast
Energy resolution	High	Medium	High	High
Temperature sensitivity	Low	High	Medium	Low
Ambient light immunity	Yes	Yes	Yes	No
Magnetic resist	Yes	Yes	Yes	No
Compact & Weight	Yes	Yes	Yes	No

The list in table 4 is further broken down in table 5[55]–[57][58] to show a more in-depth review of detectors that are within or near the optical wavelength of the transmitter used in this research.

Table 5. More in-depth observation of detectors.

Photo detector	Wavelength (nm)	Responsivity (A/W)	Dark Current (nA)	Raise Time (ns)
Silicon APD	190-1100	0.24-70	0.05-90	0.4-45
Silicon PN	580-850	0.41-0.7	1-5	5-10
Silicon PIN	850-950	0.6-0.8	10	0.070
Silicon PM	350-1000	5.2 x 10^4-2.4 x10^5	0.52-1.5 micro(s)	0.49-1.5
PMT	350-850	1.8 x 10^5-5.2 x 10^5	1-10	1.4-4.4
InGaAs PIN	1310-1550	0.85	0.5-1.0	0.005-5
InGaAs APD	1310-1550	0.80	30	0.100
Germanium	1000-1500	0.70	1000	1-2

Silicon APDs, PIN and PNs are closer related to the operating wavelength, have a responsivity and rise times. MPPCs, PMTs[59], CCDs (Charged-coupled devices), and not considered in this application despite their ability to detect single photons with very high precision because, they don't operate in the wavelength that is being used for this specific research, and they are very expensive. However, Silicon PMs can be used despite them not having any peak performance in the wavelength used. The reason for this is their

high gain factor and photosensitivity. Figure number 2 below can show a graph of an APD in comparison with a SiPM[60].

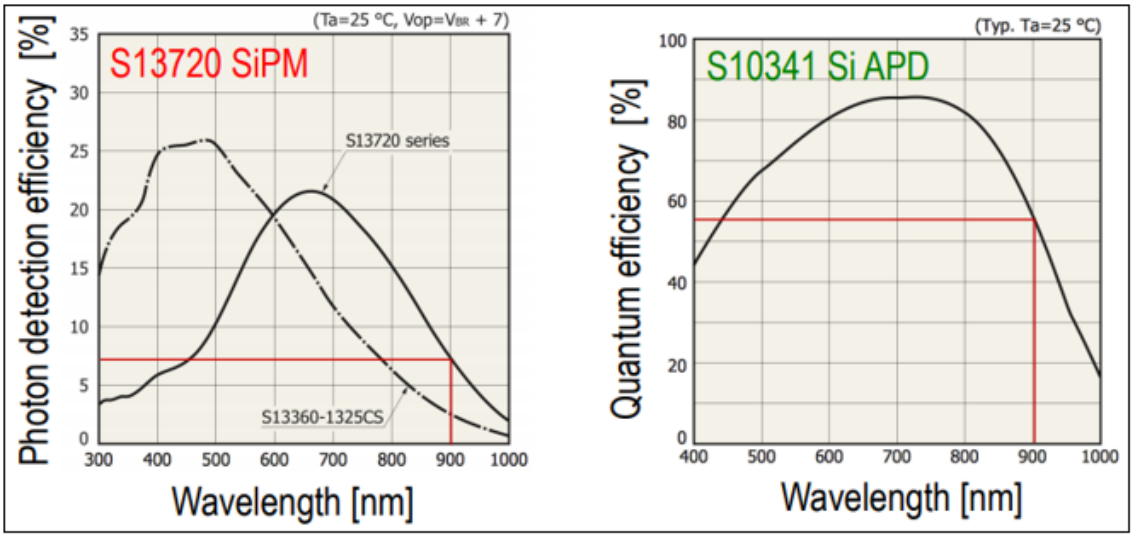

Figure 2. SiPM vs APD

From every 4 photons sent, it should be possible to receive at least 1 based on figure 3 using the SiPM. However, it should be noted that the Si APD has a good quantum efficiency at its peak wavelength too. This comparison shouldn't be confused as a fair comparison of the 2 components. Quantum efficiency is not equal to photon detection efficiency.

3.1.1 PIN diode sensors

A P–I–N photodiode, also called PIN photodiode, is a photodiode[61][62] with an intrinsic (I) also known as an undoped region in between the N- and P-doped regions. Most photons are absorbed in the intrinsic part of the diode, and carriers generated therein can efficiently contribute to the photocurrent[62]. In Figure 3, the electrodes are shown in black: the cathode is a flat electrode, whereas the anode has a ring form (of which two opposite parts are seen in the illustrated cross-section). The cathode is connected to the positive pole of the reverse bias voltage. On top of the p region, there is an anti-reflection coating(green).[62][63]

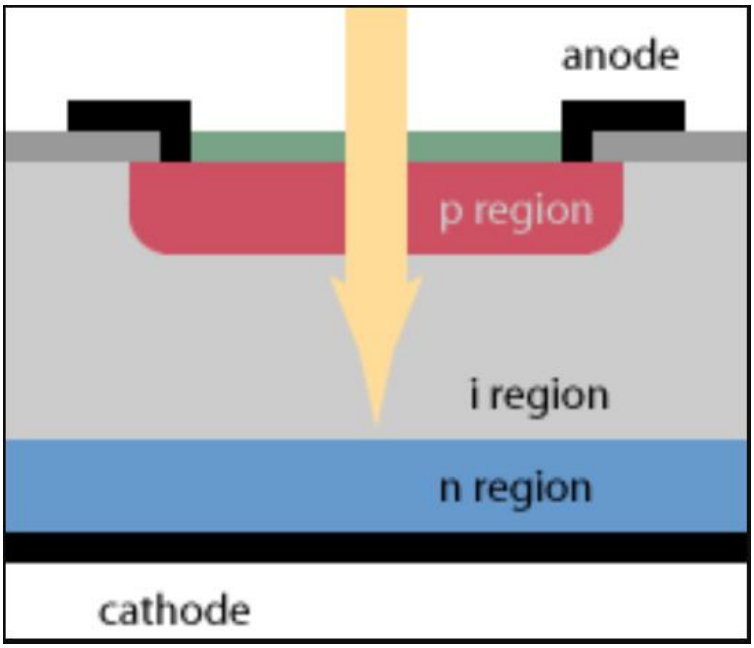

Figure 3 Schematic drawing of a P–I–N photodiode.

3.1.1.1 Why PIN photodiodes

Typically, PIN photodiodes are fast. Ordinary P and N photodiodes are prone to have the following problems[62]:

- The area of the depletion region can be well below the absorption length, so that generation of only some fraction of the generated photocarriers is within the depletion region. The collection of the carriers generated outside the depletion region may be limited, leading to a reduced quantum efficiency.[62]

- Carriers created outside the depletion area which eventually diffuse into the depletion area and add to the photocurrent, that dispersion takes some time; the outcome is a queue in the impulse response, which can restrict the recognition data transfer capacity [62].

These problems are avoided with P–I–N photodiode design where the generation of carriers is performed in the intrinsic region because that can be much thicker than the depletion region of a P–N structure. Another effect of the dense intrinsic area can be the reduced capacitance, which allows for a higher detection bandwidth.[62]

Some P–I–N diodes are made from different semiconductor materials, where the bandgap energy is below the photon energy only for the intrinsic region, but not for the P and N regions. In that case, any absorption outside the inherent area can be avoided.[62]

The fastest P–I–N photodiodes have bandwidths well above 100 GHz, and the reactive surface of these photodiodes only covers a diameter of a few microns. They are often made in fiber-coupled form and can be applied, e.g., in receivers for optical fiber communications; the achieved bit rates can be as high as 160 Gbit/s.[62]

3.1.2 Avalanche Photodiodes (APD)

Avalanche Photodiodes just like PIN photodiodes work as photoreceiver. Their properties, however, make them more superior than PIN photodiodes when it comes to sensitivity. Their principle of operation is slightly different than that of PIN diodes. The incoming photons trigger a charge avalanche internally. The only requirement here is to widen the absorption layer by applying a reverse bias voltage.[64] Figure 4 below shows how an avalanche photodiode is structured broken down into layers.

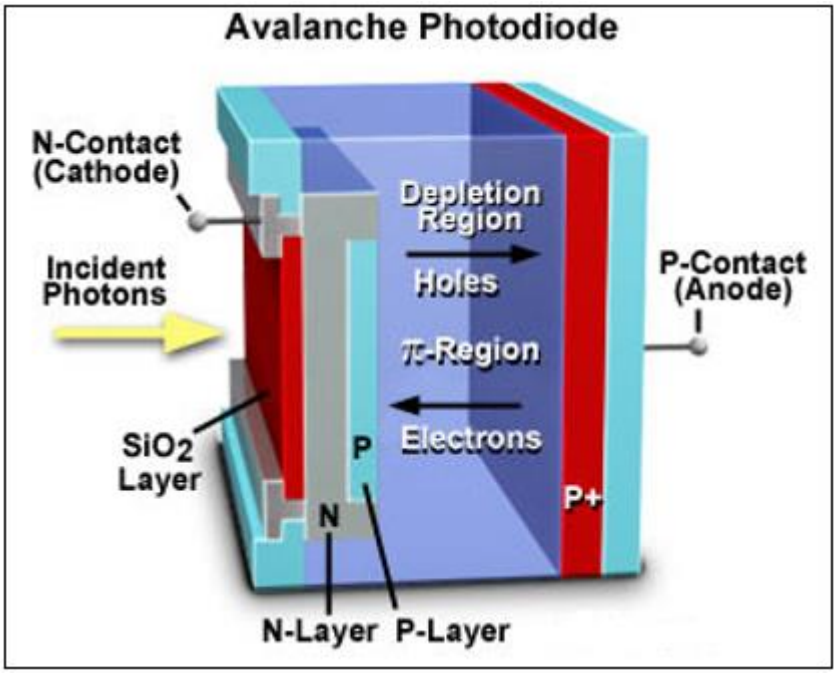

Figure 4. Avalanche photodiode layers

Avalanche photodiodes are more superior than PIN photodiodes when it comes to sensitivity. The gain of an APD is increased many times by the avalanche action which provides its superior sensitivity. This, however, means that APDs require higher operating

voltages compared to PIN photodiodes as seen in table 4. As a result, APDs output nonlinear signals and a great deal of noise.

For avalanche multiplication of the holes and electrons created by the initial electron-hole pair to occur, APDs require high reverse bias currents, contrary to PINs. The internal region where electron multiplication occurs by applying an external reverse voltage gives APDs more gain in the output signal which lets them measure low lights at high speeds.

There is a different way or modes to connect an APD. Figure 5 below shows the Geiger and Linear mode

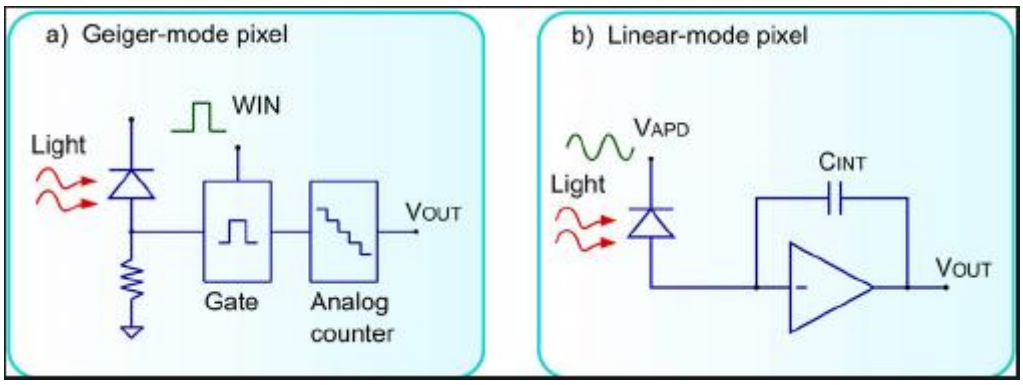

Figure 5. Connecting an APD

The difference between the Geiger and linear modes is, the linear mode is typically used in single pulse systems, single detection, and slow sample rates. Geiger mode, on the other hand, offers a large array of collection, collection from multiple angles and a high sample rate.[65]–[67]

3.1.3 Silicon Photomultipliers (SiMPs)

SiMPs are based on single-photon avalanche photodiode sensors (SPADs). Each SPAD has its own quenching resistor as shown in figure 6 below[68], each independently operating SPAD with its quenching resistor is called a microcell. Once a microcell within a SiPM outputs in response to an absorbed photon, a Geiger avalanche is started, which makes the photocurrent flow through the microcell. This causes a voltage drop on the quench resistor which reduces the bias across the diode to a nominal below breakdown, which results in quenching the photocurrent and avoid more Geiger mode avalanches from occurring. After the quenching is completed, the voltage across the diode recharges to the nominal bias value. The process of recharging until full functionality is what is referred to as recovery time. While the avalanche process is happening, all other

microcells remain ready to detect photons. This means the Geiger avalanche process in one micro does not spread to others.[68]

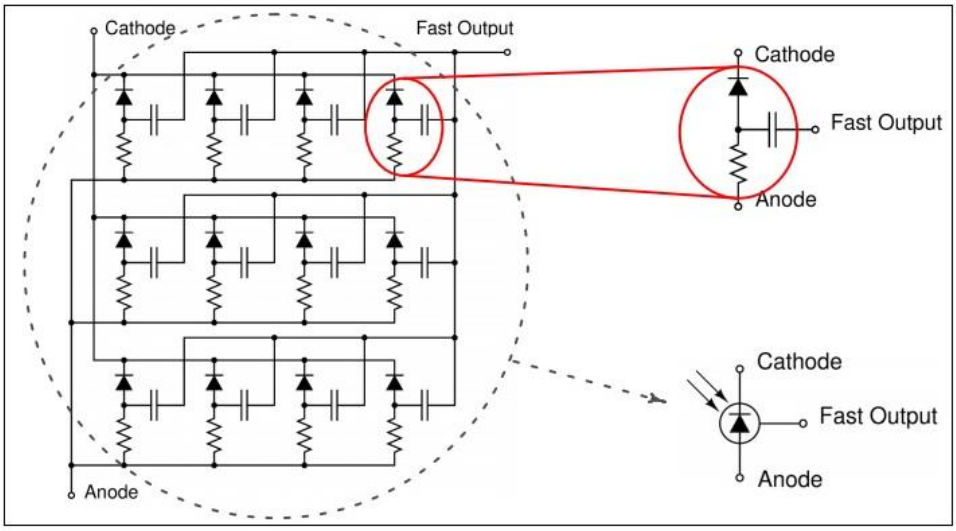

Figure 6. SiPM microcells

3.2 Biasing

A photodiode is a current generator. So, its junction capacitance is dependent on the depth of the depletion layer. Depending on the design requirements of the photodiode, a biasing voltage is provided either on the cathode or the anode (reverse bias or forward bias) to decrease or increase the depletion region. This in return increases the gain of a photodiode or SiPM. Photodiodes are generally reverse biased but it's also possible to operate them with zero bias.[69] when a photodiode is forward biased, then the creates current within the sensor. If there is already high current within the sensor and more current is generated due to photon detection, the generated current (useful signal) will be hard to measure. But if reverse bias is used, then almost no current is flowing through the sensor hence making it easier to measure any current generated with light detection.

3.3 Receiver Choice

Silicon PIN (SiPIN) diodes are fast with a very short rise time as compared to Silicon APDs (SiAPD). But SiAPDs are more sensitive than SiPIN and for this application, it's sensitivity over speed since the received signal is very week hence going with Silicon Photomultipliers (SiPM) for their superior sensitivity in the optical wavelength window the experiment is to be conducted.

Specifically, ON semiconductor's MICRORB 10035 SiPM with dual outputs, the fast output has a capacitance of 1pF and the standard output has 100pF. Its properties such as responsivity and high gain make it the choice for this purpose. Some details in table 5 below. More details in the datasheet.[68]

Table 6. MICRORB 10035 SIPM

Parameter	10035	Unit
PDE @ 905 nm @ Maximum Overvoltage	10.3	%
PDE @ 905 nm @ Typical Overvoltage	9.1	%
Responsivity @ 905 nm @ Maximum Overvoltage	420	kA/W
Responsivity @ 905 nm @ Typical Overvoltage	240	kA/W
Gain − Cathode-anode Output	1.7 × 10^6	
Dark Count Rate	2.6	MHz
Dark Current	1.5	Micro A
Rise Time − Standard Output	0.9	ns
Microcell Recharge Time Constant	73	ns
Rise Time − Fast Output	490	ps
Fast Output Pulse Width (FWHM)	3.7	ns
Crosstalk	43	%
After pulsing	1	%
Excess Noise Factor	1.22	

4 Design and assembly

The results got here will be used to model the hardware later. The transmitter is out of the scope of this thesis, so it won't be covered, but it's crucial to at least understand what kind of transmitting element (IrLD and IrLED)s to adjust and tune out the receiver to their wavelength. The location of the Transmitters can be seen in figure 7 below which shows a mock version of the TTU 100 satellite.

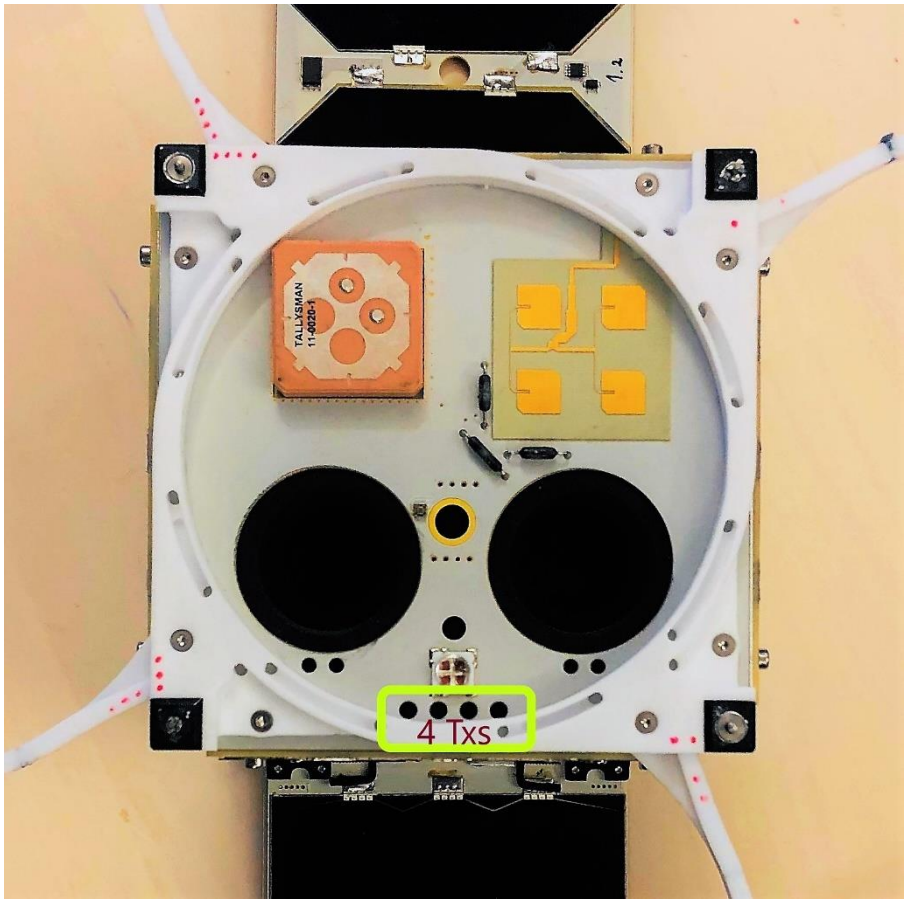

Figure 7. The bottom section of the satellite showing the 4 IR TXs

The 4 TXs are Panasonic's LNCT22PK01WW MOCVD fabricated 660 nm and 785 nm band dual wavelength laser diodes with multi-quantum well structure[70] as the transmitting element.

4.1 Receiver calculations

4.1.1 Optical divergence

One of the main challenges I need to overcome is the signal divergence with distance. The LNCT22PK01WW infrared laser diodes used in the transmission are connected in parallel with each. The IrLEDs have a typical perpendicular divergence angle of 15 degrees and 7.5degrees parallel divergence. Figure 8 below shows how a beam will spread over distance.

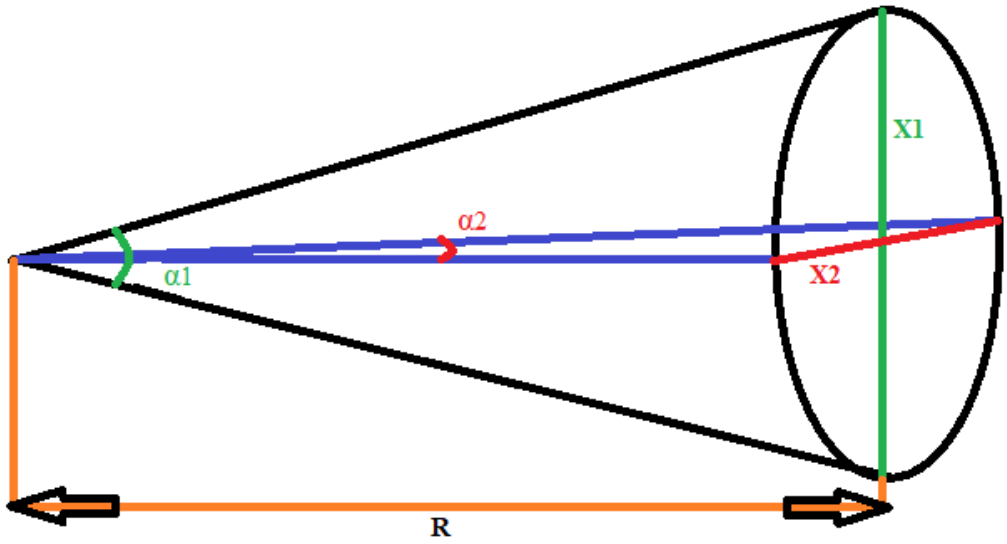

Figure 8. Optical spread after a given distance

Angle α1 = 15 degrees

Angle α1 = 7.5 degrees

Range "r" = 500 km

I need to find x1 and x2

$$x = r \times a \frac{\pi}{180} \quad (9)$$

Or

$$x = 2 \times r \times tan(a/2) \quad (10)$$

Using equation 9:

$$x1 = 500000 * 15 \frac{\pi}{180} = 131652m$$

X2 =65543m

$$x1 = 500000 * 7.5\frac{\pi}{180} = 65543m$$

Based on the calculations above it can be determined that the link will radiate and elliptic-like a signal on the ground covering an area of about 131 km by 65 km on the elliptic axes.

Now that x1 and x2 are known, can go ahead and find the area of the radiated area which can be found using the area of an ellipse equation.

$$A = \pi ab = \pi * 65826 * 32771 \approx 6 * 10^9 m^2$$

4.1.2 Scattering coefficient results

Using equation 1, I can find the scattering with respect to the wavelength.

$$scattering = \frac{3.91}{Range}\left(\frac{lmd}{550nm}\right)^{-q}$$

Scattering coefficient = 13.8

4.1.3 Atmospheric attenuation results

Using this equation 8, and factoring in all the parameters,

$$T(R) = \log e^{\left(\left(\frac{3.91}{Visibility}\right)*\left(\frac{lmd(nm)}{550nm}\right)^{-q}*R\right)} dB$$

the atmospheric attenuation is 0.839 dB.

4.1.4 Received power results

To get the power of the received signal, there are a few factors that need to be considered such as transmitted power, atmospheric loss, the transmission length or the distance between the transmitter and receiver, the angle of divergence (for the laser diode) and the area of the receiver (receiving surfaces). Using equations 3 in chapter 2.4.2, an estimate of power at the receiver can be made.

$$\Pr(dBW) = Pt + Gt + Gr + S$$

By expanding equation 3,

$$\Pr(dBW) = Pt + \left(\frac{16}{\theta a.\theta b}\right) + \left(\frac{\pi dr}{\lambda}\right)^2 + \left(\frac{\lambda}{4\pi R}\right)$$

$$\Pr(dBW) = 0.80 + \left(\frac{16}{13 * 7.5}\right) + \left(\frac{\pi * 0.3048}{785 * 10^{-9}}\right)^2 + \left(\frac{785 * 10^{-9}}{4 * \pi * 500000}\right)$$

$$\Pr(dBW) = -1.93 + (-7.84) + 121.72 + (-258.06)$$

The above gives approximately -146.11 dBW which is -116.11 dBm as power received.

Link margin

Link margin refers to the actual difference between the sensitivity of the receiver and expected minimum power. In other words, it can refer to how much room for error, signal or power degradation a communication system can have before it can't receive useful information. It is measured in decibels. The power link margin is dependent on the transmitted power, in this case, the laser power, receiver sensitivity, receiving surface area size and FOV, [71]as well as beam divergence.

Link margin = Pt + Sr – Total Att

Pt here is transmitter power and Sr is receiver sensitivity. Total Att, however, in this case, can vary from condition to condition. It comprises of values carried by atmospheric, geometrical, rain, scintillation snow, fog attenuations, and any other forms.

4.1.5 Link Budget

Calculations about the transmitter and receiver gains, propagation losses, scattering and other factors that can affect this system will be covered in this part. Table 6 below will give some specs relating to this FSO system.

Table 7. FSO Parameters

Parameters	Values	Units
Range	500	km
Wavelength	785	nm
Tx power (max)	800	mW
Beam divergence	13 and 7.5	deg
Signal footprint	131 by 65.54	km
Received power	-116.11	dBm
SNR	19	dB
BER	10^{-5}	-

The bit error rate (BER) and signal to noise ratio (SNR) can be found in chapter 4.2.2

4.2 Receiver Design

Cube satellites have space and weight power consumption limitations, so the installation of a high-performance transmitter is not possible. supposed to be as simple as possible with variables such as power consumption, weight and occupied space in mind, which in reverse means that all the complication is done in the receiving end. So, the complete receiver will be a combination of both sophisticated hardware and software. Figure 9 below shows an ideal FSO communication system architectural representation.

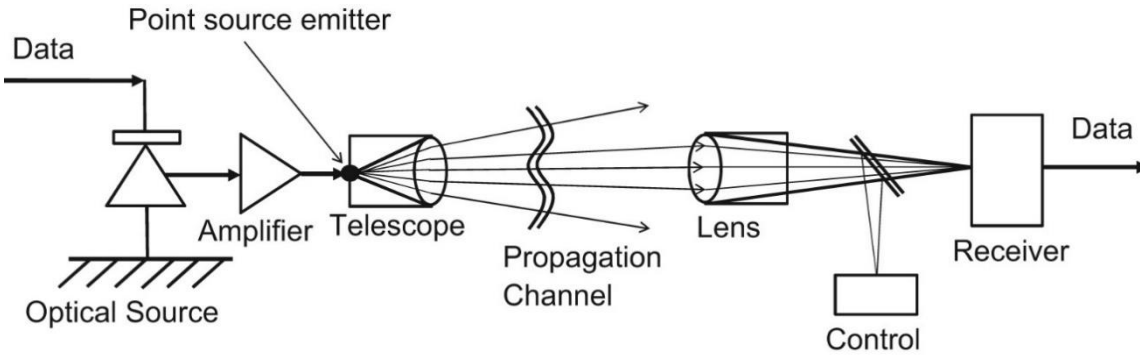

Figure 9. FSO transmitter and receiver design architecture

4.2.1 Operating principle

Contrary to Figure 9, the receiver uses a catadioptric telescope for the optics. This type of telescope has two mirrors as shown in figure 10. The primary mirror is bigger than the secondary mirror, and it's parabolic in shape. Its design allows it to collect light rays and reflect them onto the secondary mirror which bounces them through a tube to the eyepiece.

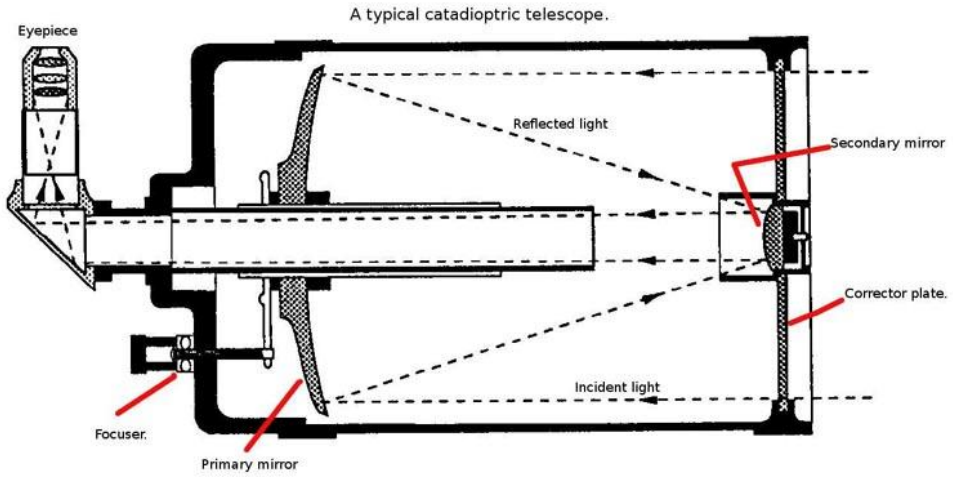

Figure 10. A catadioptric telescope

In my design, I'll get rid of the eyepiece and instead mount photo sensors there such that, when the light comes from the secondary mirrors, it falls directly onto the optic sensors. The optical sensors will then convert the light into a current signal that will be sent into a current to voltage converter, typically an OpAmps.

4.2.2 Hardware

To build this kind of receiver, I need very high sensitivity elements with a shallow noise floor.

- Amplifier
- ADC
- Silicon photomultiplier
- STM32F4 discovery board
- Meade's LX90 telescope

SiMP output

Knowing the sensor (microrb 10035) and received power (-116 bBm), the sensor output current can be calculated by multiplying the sensitivity in A/W with the received power in amperes. The received power in amperes is approximately 2.44 femtoamperes. The receiver sensitivity is 420 KA/W. So, 1 nA will be the output current of the SiMP

Amplifiers

The amplifier design can affect system performance. It's important to find an amplifier with extremely low noise, high gain, and high input impedance. In this part, different architectures and types will be analyzed to choose which type to use with the SIPM and input stage of the ADC.

Charge amplifiers (integrator)

Charge amplifiers are low noise FET with high open loop gain so that its amplification is not influenced by the detector's capacitance. Detectors sometimes produce a weak charge pulse with a width of several tens of nanoseconds. Detectors usually have very high impedance since the sensitive element itself is capacitive.[72], [73] The above properties must be taken into consideration when choosing the right device to amplify the output signal of the detector. This is where operation amplifiers using a feedback capacitor

(integrator mode) are commonly used. These amplifiers integrate weak charge pulses and convert them into voltage pulses for amplification then give a low impedance output, they also have high input impedance. Figure 11 below shows a schematic of a charge amplifier and detector.

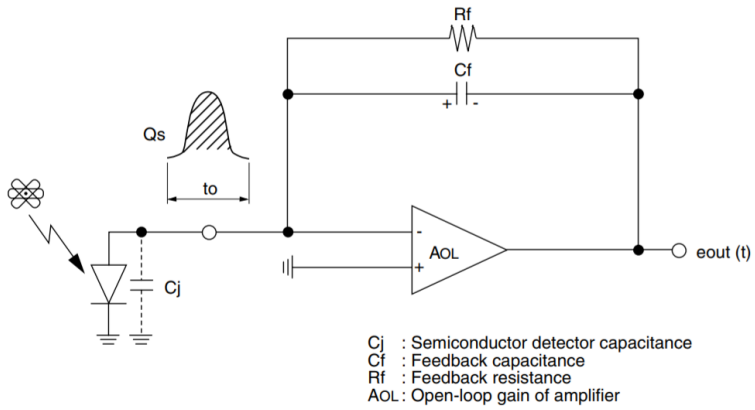

Figure 11. Charge Amplifier

Transimpedance operational amplifier

Designing high-resolution detection circuits using photodiodes presents considerable challenges because of bandwidth, gain, and input-referred noise is coupled together[74]. The purpose of a transimpedance circuit is to convert an input current from a current source (typically a photodiode) into an output voltage. However, the factors below limit the possible gain while using this method [74]:

- The current source input impedance;
- The load impedance; and
- Desired bandwidth.

Figure 12 shows a suitable circuit with all components for achieving the needed results. In this circuit, the signal source is a photodiode, whose role is to convert the photons into a photocurrent. The feedback resistor then amplifies this current R_F. Working with an ideal amplifier for now, we can see that because no bias current is present, all the signal generated by the photodiode is going to be converted to the output. Note that the source impedance is not of interest here. Note also that the output is low impedance, allowing a wide variety of load to be connected. The bandwidth is a function of the source

capacitance (C_S), the feedback capacitance (C_F), and the gain bandwidth product of the actual amplifier used[74].

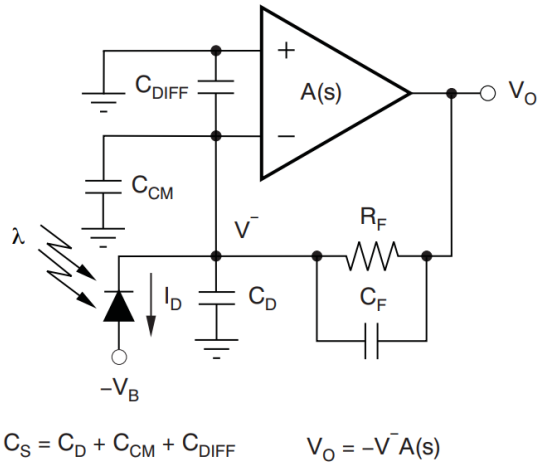

Figure 12. Transimpedance Circuit with Modelled Elements

The source capacitance (C_S) is the sum of the photodiode capacitance (C_D), the common-mode capacitance of the amplifier (C_{CM}), and the differential capacitance of the amplifier (C_{DIFF}). C_{CM} and C_{DIFF} include both the board layout and the op amp parasitic capacitance[74].

Instrumentation Amplifier

This is a type of differential amplifier with a very high gain, common mode rejection ratio (CMRR) and high input impedance. It is applicable in systems with very weak signals and places where impedance matching is very important. Figure 13 below shows how an instrumentation amplifier looks like.[75] The high CMRR and open loop gain give instrumentation amplifiers an edge over other amplifiers. These amplifiers are typically used in low-level transducer amplifiers, high impedance transducers, capacitive sensors, multi-channel data acquisition and so on. The similarity between most of these applications is the presence of a very week signal almost close to the noise floor. This is where high CMRR is useful[75]. Since it's a differential amplifier, it amplifies the difference between the 2 inputs signal voltages or currents and rejects any signals that are common between both inputs. Therefore, it's very useful in the extraction of tiny signals from transducers and other signal sources.[75]

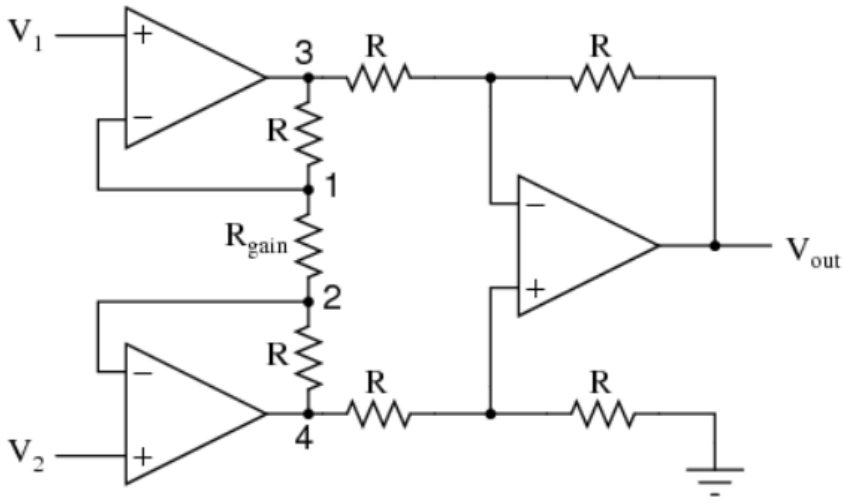

Figure 13. Instrumentation Amplifier

Operational Amplifier (OpAmp) used

After looking at the different op-amp architectures, the trans-impedance architecture was selected.

Specifically, linear technology's LTC6240.[76] It's an 18MHz low noise, rail to rail output CMOS op-amp. Since the design has very low bandwidth requirements, this opamp is well suited for the job due to its small bandwidth and unity gain which mean less noise towards the cut off frequency and is optimized to work in the small bandwidth range [76] More details in the datasheet.

Amplifier Calculation and component value selection

The key main parameters to watch out for in this design are: feedback resistor or commonly known as a gain resistor, feedback capacitor, and the gain bandwidth. The feedback capacitor will directly impact on the amplifier circuit's bandwidth.

Feedback resistor

To select the feedback of the gain resistor (resistor R_F in figure 12), the equation below can be used.

$$R_F = \frac{V_{out\,max} - V_{out\,min}}{Input_{imax}} \quad (11)$$

$V_{out\,max}$ in this equation is the maximum voltage which is determined by the input of what needs to be driven. $V_{out\,min}$ could be 0 in ideal conditions depending on the input.

$Input_{imax}$ is the current from the sensor (SiPM). Knowing the current output of the sensor (1nA), RF can be approximated to be in the Giga Ohms range. Such an amplifier will have a very small bandwidth so optimization will be required and there will be a need to more than 1 amplification stages figure 14 below shows the optimised first stage.

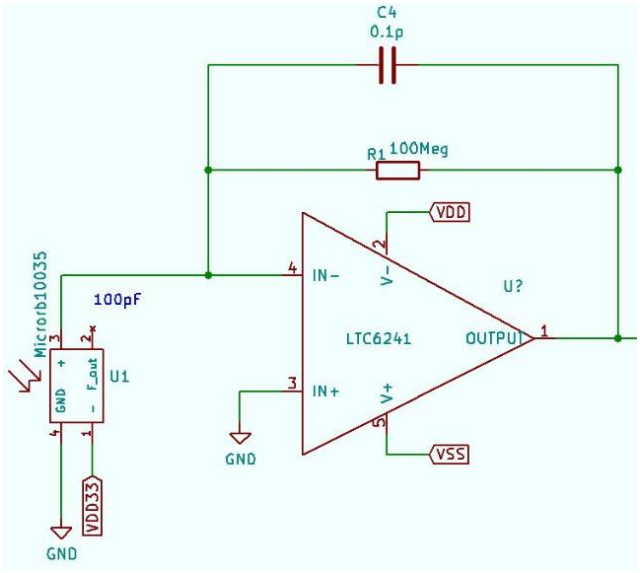

Figure 14. Optimization and First stage

To be able to archive the 10 kbps requirement in the task specification (1.2), optimization is done using a 100M Ohm resistor instead of a Giga Ohm range resistor.

Feedback Capacitor

The feedback capacitor C_F according to figure 12 can be calculated using the formula below but due to the signal level and optimization done, a 0.1pF capacitor is selected as seen in figure 14 above.

$$C_F \leq \frac{1}{2*\pi*R_1*f_p} \tag{12}$$

Gain bandwidth

To calculate the gain bandwidth, equation 13 below can be used knowing C_f and R_F.

$$Gain\ BW = \frac{C_{input}+C_F}{2*\pi*R_F*{C_F}^2} \tag{13}$$

From this equation 14, C_{input} is the total input capacitance which is the sum of input source capacitance C_s + C_{diff} which is the differential input capacitance of the amp + C_{com} which is the common mode input capacitance of the inverting inputs. The value of C_{input} is in Farads. C_F and R_F are already known. The results will be in Hertz. Using the formula above, the gain bandwidth is 16.5 MHz.

Cut off Frequency

The cut off frequency is dependent on the feedback capacitor C_F and the feedback resistor R_F. This is the frequency at which the power in a system begins to reduce also known as the -3dB frequency (the frequency where the magnitude response is 3dB lower than 0 Hz). This can be calculated using the equation 14 below

$$F_p = \frac{1}{2*\pi*R_F*C_F} \tag{14}$$

The values of C_F and R_F are known so F_p is 15.9 kHz.

Figure 15 below will show the frequency response of the feedback RC path of the amplifier used.

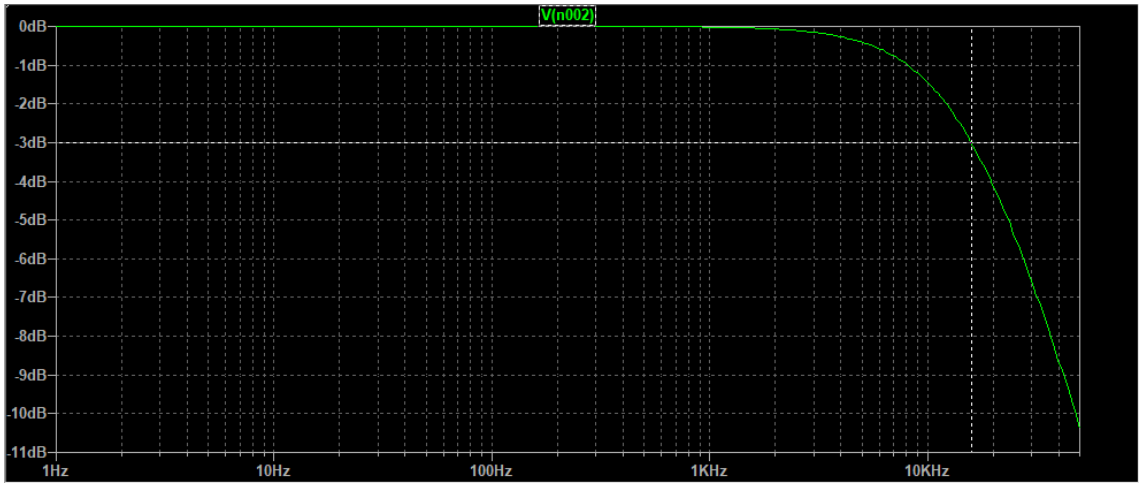

Figure 15. Cut off frequency and Response

The SiMP has a dark current of 1.6 uA this dark current is bigger than the input signal and needs to be canceled out. To do that, an integrator circuit is used. which is shown in figure 16 below.

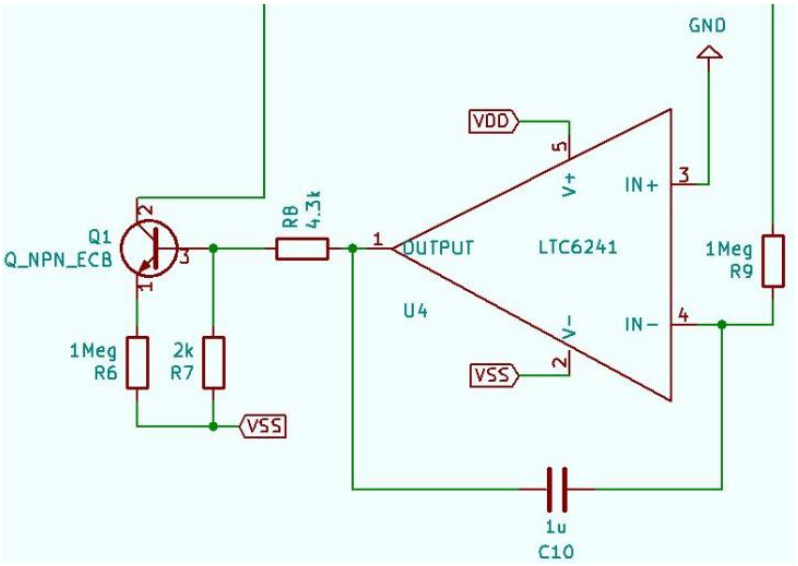

Figure 16. Integrator circuit

The integrator has a -3.21 voltage output that opens the NPN transistor which supplied with a negative voltage which creates a negative current which compensates the dark current at the input by canceling it out and background light with a time constant of 1s. With this stage done, the output of the first stage is about 100 mV. To utilize the dynamic range of the ADC, it requires an input of about 1 to 2 volts. So the 100 mV would need to be amplified at least 10 times. The second stage amplifier is shown in figure 17 which puts out 1 V leaving some headroom in case of any spike in the input power.

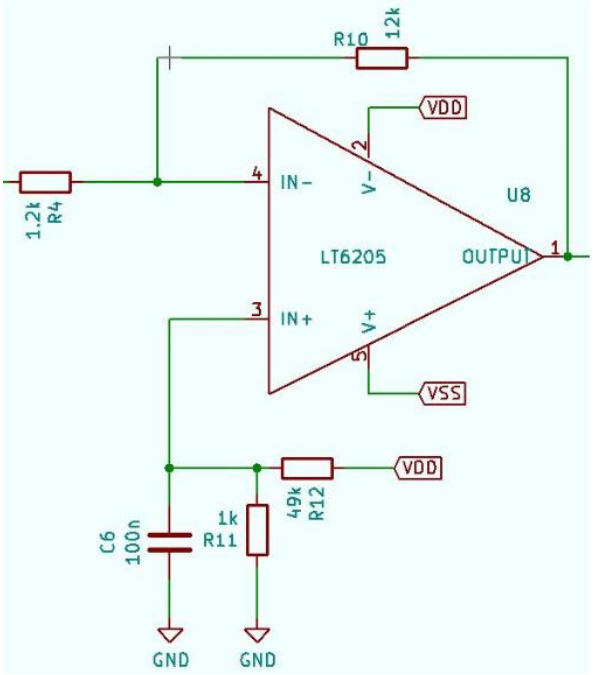

Figure 17. second stage

The complete schematic is in appendix 2.

Transimpedance SNR

To get the SNR, I sum up the RMSs of different noise sources such as the voltage noise, current noise, and resistor noise. These can be found using:

$R_f = 100M\Omega$ Feedback resistance

$C_f = 0.1pF$ Feedback capacitor

$C_j = 100\ pF$ Photodiode junction capacitance (from photodiode manufacturer)

$C_{opa} = 3.5\ fF$ Op-amp input capacitance (LTC6240 data sheet)

$C_i = C_j + C_{opa}$ Total input capacitance

$f_c = 18\ MHz$ Unity gain bandwidth (in the LTC6240 datasheet)

$f_p = \frac{1}{2\pi R_f \cdot C_f} = 15.9\ kHz$ Transconductance bandwidth

$f_z = \frac{1}{2\pi R_f \cdot (C_i + C_f)} = 15.4\ Hz$

$f_i = \frac{C_f}{C_i + C_f} \cdot f_c = 17.4\ kHz$

$e_{nif} = 7\frac{nV}{\sqrt{Hz}}$ Broadband noise spectral density (LTC6240 data sheet)

$f_L \coloneqq 0.1\ Hz$ Lower bound on frequency (1/f region) (arbitrary lower bound of frequency)

$e_{at\_f} \coloneqq 60\frac{nV}{\sqrt{Hz}}$ Flicker noise measured at f_L (LTC6240 data sheet noise curve)

$e_{fnorm} = e_{at\_f} \cdot \sqrt{f_L} = 19\ nV$

$f_f = \frac{e_{fnorm}^2}{e_{nif}^2} = 7.35\ Hz$

voltage Noise calculation

$E_{noe1} = \sqrt{e_{nif}^2 \cdot f_f \cdot \ln\left(\frac{f_f}{f_L}\right)} = 39.3\ nV$

$E_{noe2} = \sqrt{e_{nif}^2 \cdot (f_z - f_f)} = 19.8\ nV$

$E_{noe3} = \sqrt{\left(\frac{e_{nif}}{f_z}\right)^2 \cdot \left(\frac{f_p^3 - f_z^3}{3}\right)} = 528\ \mu V$

$E_{noe4} = \sqrt{\left(e_{nif} \cdot \frac{C_i + C_f}{C_f}\right)^2 (f_i - f_p)} = 277\ \mu V$

$E_{noe5} = \sqrt{\frac{(e_{nif} \cdot f_c)^2}{f_i}} = 956\ \mu V$

$E_{noe} = \sqrt{E_{noe1}^2 + E_{noe2}^2 + E_{noe3}^2 + E_{noe4}^2 + E_{noe5}^2} = 1.3\ mV$ (total voltage noise)

Each form noe1to 5 corresponds with a different area in the voltage output noise curve.

Current Noise calculation

$k_b \coloneqq 1.38 \times 10^{-23}$ J/K Bolzmann constant

$T_n \coloneqq 298$ K Temperature in Kelvin (289K = 25℃)

$R_{sh} \coloneqq 30M\Omega$ Shunt resistance of SiPM

$i_j = \sqrt{\frac{4 \cdot k_b \cdot T_n}{R_{sh}}} = 10.472 \ \frac{pA}{\sqrt{Hz}}$ Thermal (Johnson noise)

$q \coloneqq 1.602 \times 10^{-19} \ C$ One electron charge

$I_D = 1.6 \ \mu A$ Dark current of SiPM

$i_{sL} = \sqrt{2q \cdot I_D} = 693.2 \ \frac{fA}{\sqrt{Hz}}$ Shot noise (dark)

$I_L = 0 \ A$ Photo current in photodiode (our measurements are dark)

$i_{sD} = \sqrt{2q \cdot I_L}$ Shot noise (white light)

$i_{n\_diode} = \sqrt{i_j^2 + \ i_{sD}^2 + \ i_{sL}^2} = 693.6 \ \frac{fA}{\sqrt{Hz}}$ (Total diode current noise)

Resistor Noise calculation

$K_n = 1.57$ the coefficient first order low past filter

$BW_n = K_n \cdot \ f_p$ Noise bandwidth (brick wall filter)

$e_{n\_r} = \sqrt{4k_b \ \cdot \ T_n \ \cdot \ R_f \ \cdot \ BW_n} = 203 \ \mu V$ Thermal noise at output

$i_{n\_opa} = 0.56 \ \frac{fA}{\sqrt{Hz}}$ Noise current from LTC6240 data sheet

$i_{n\_diode} = \sqrt{i_{n\_opa}^2 + \ i_{n\_diode}^2} \ \frac{A}{\sqrt{Hz}}$ (Total noise current)

$K_n = 1.57$ Moise bandwidth factor first-order filter

$BW_n = K_n \ \cdot \ f_p = 25 \ kHz$ Noise bandwidth (brick wall filter)

Total Noise calculation

$E_{noi} = i_{n\_total} \ \cdot \ R_f \ \cdot \sqrt{BW_n} = 11 \ mV$ Current noise at output

$E_{noe} = 112 \ \mu V$ OP-amp voltage noise

$E_{n\_R} = 203 \ \mu V$ Resistor noise

$E_{noI} = 11\ mV$ Op-amp current noise

$E_{no} = \sqrt{E_{noR}^2 + E_{noI}^2 + E_{noe}^2}$ = 11 mV Total output noise for Ltc6240 transimpedance amp

Using equation 4, SNR = 100/11 = 9 which is approximately = 19dB.
According to the paper named a power analysis model for outdoor long-distance visible light communication[77], [78], a 19dB SNR is more than sufficient for OOK to work as shown in figure 18.[77], [78]

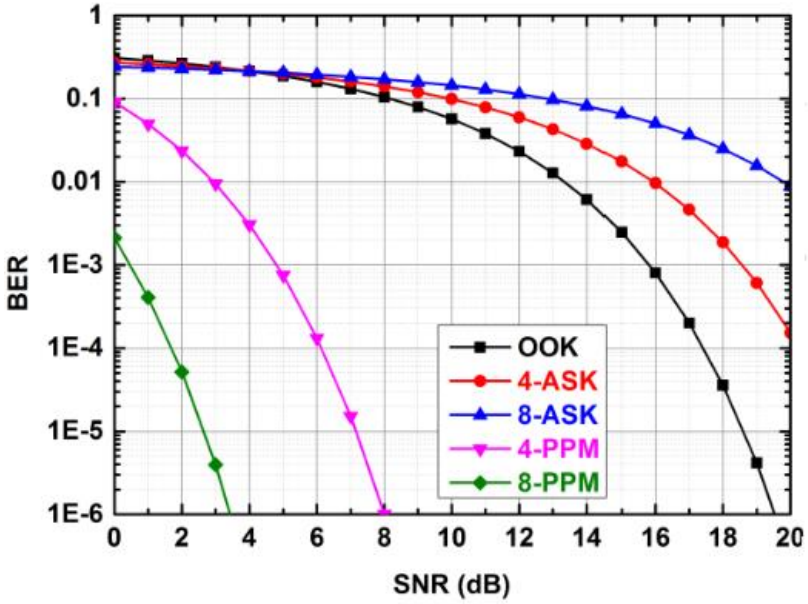

Figure 18. SNR vs BER for different modulations

Background light elimination

APDs usually have a big wavelength spectrum coverage. This big coverage is bound to raise the noise floor in the communication system. With the received signal fluctuating due to changing atmospheric conditions, it's important to filter out the unwanted wavelength and concentrate the receiver in the needed spectrum range. The first stage can be done using optical filters such as what's shown in Figure 19 below. [79] These optical filters attenuate the unwanted light and only allow the needed spectrum.

Figure 19. Optical filters

The graph below in Figure 20 [80]will show signal behavior when the optical bandpass filters in Figure 19 are used and when not used.

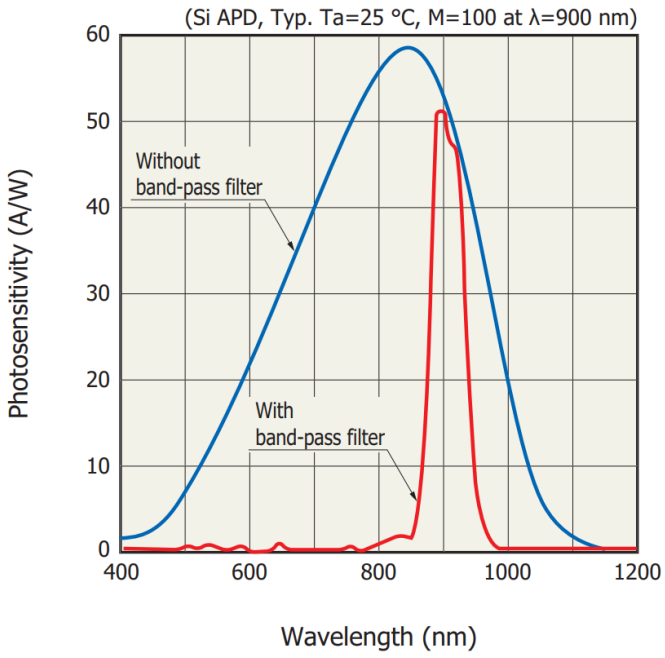

Figure 20. With and without optical filters

Analog to digital converter (ADC)

There are 4 known types of ADC architectures:

- Delta-sigma (▲Σ)
- Pipeline

- flash
- Successive Approximation Registers (SAR)

The delta-sigma ADC rely on oversampling and digital filtering to perform well and archive high accuracy. For them to work well however, they require that the input signal doesn't change faster than the sampling rate which simply means that they require stability. They are slower than the SAR architecture but can attain higher resolutions and accuracy.

The SARs, on the other hand, perform input signal sampling and use an iterative process. Each bit of resolution requires at least one successive comparison due to the use of a single comparator. The result is temporarily stored in an on-chip register.

Contrary to other ADCs, the pipeline converters use undersampling, multiple stages, larger cycle-latency, sample and gain algorithm topology to perform. They are the fastest of all being 10 to 40 times faster than the SAR devices. The trade-off here however is, they have very low resolutions and high-power consumption. They have high input capacitance which results in low source impedance is required to aid the settling time and a buffer may be required for this architecture to isolate the source resistance and capacitance. Figure 21 below shows the practicality of each ADC architecture.

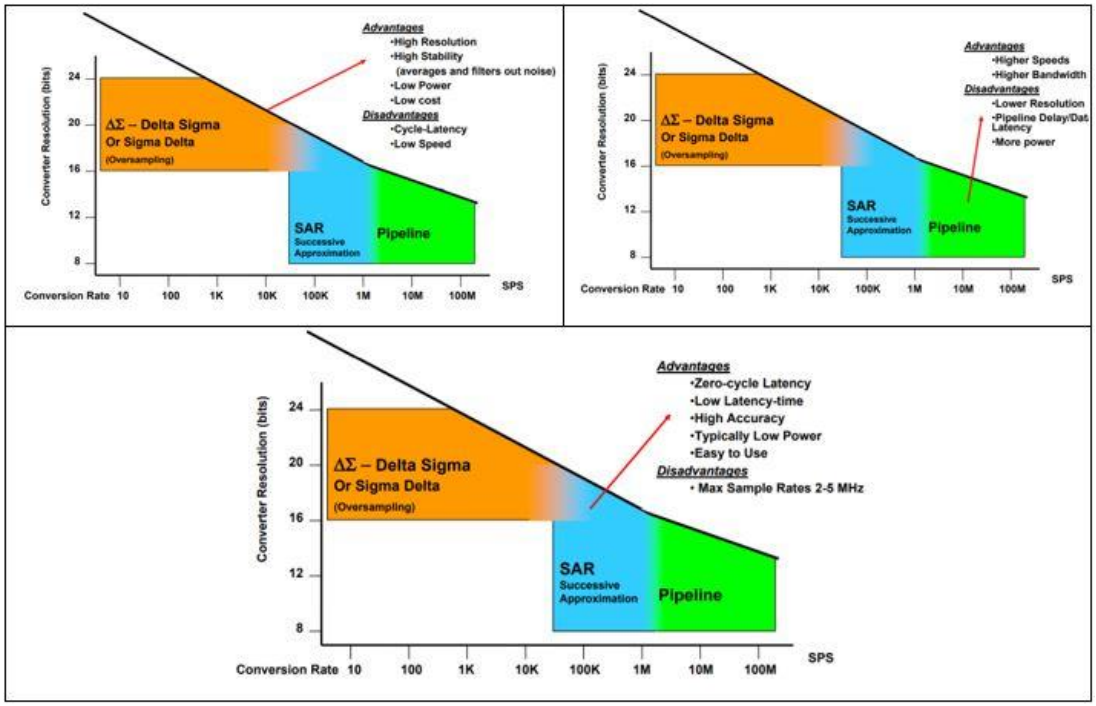

Figure 21. ADC Architectures

In table 8 and table 9 below, I'll continue to compare these different types of these ADC architectures chose a type to use at the end.

Table 8. Architecture Comparison

ADC Topology	*F Conversion*	*Resolution*	*Comments*
SAR	≤ 4Msps ≤ 1.25Msps	≤ 16-bit ≤ 18-bit	Simple operation, low cost, low power.
Delta-Sigma	≤ 4ksps ≤ 4Msps ≤ 10Msps	≤ 31-bit ≤ 24-bit ≤ 16-bit	Moderate cost.
Pipeline	≤ 200Msps ≤ 250Msps ≤ 550Msps	≤ 16-bit ≤ 14-bit ≤ 12-bit	Fast, expensive, higher power requirements.

Table 9. Performance Specifications

Characteristic	Pipelined	SAR	Delta Sigma
Throughput (samples/sec)	++	+	0/+
Resolution (ENOB)	0	+	++
Latency (Sample-to-Output)	+	++	0
Suitability for converting Multiple Signals per ADC	+	++	0
Capability to convert non-periodic multiplexed signals	+	++	-
Power Consumption	Scales with Sample Rate or Constant	Scales with Sample Rate	Constant

After looking through the specifications of different ADC architectures, the SAR architecture will be used for this project because of its simplicity of use and speed, of which Analog devices' AD7450 will be used.[81]

The AD7450 is a 12-bit differential ADC capable of 1Msps with an externally adjustable wide input common mode range. This ADC is used because of its high speed and dynamic range, resolution and communication interface compatible with most microprocessors.

STM32F4 discovery board

This discovery board will be used as the controller for the receiver. Many of the board functions and features are not relevant to the project functionality and will not be used. Our main interest here is the STM32F407VGT6 microcontroller that drives the board.[82]

The STM32F407xx family is built on the high-performance ARM Cortex-M4 32-bit RISC core operating at a frequency of up to 168 MHZ. The core features a floating-point unit single precision which supports all ARM single-precision data processing instructions sets and data types. It is also capable of implementing a full set of DSP instructions and also has a memory protection unit which enhances application security.[82]

The STM32F407xx family comes embedded with high-speed embedded memories. (A Flash memory of up to 1 Mbyte and up to 192 Kbytes of SRAM), it also comes incorporated with up to 4 Kbytes of backup SRAM, and an extensive range of enhanced input-output ports and peripherals connected to two APB buses, three AHB buses, and a 32-bit multi-AHB bus matrix.[82]

All devices offer three 12-bit ADC, two DACs, a low-power RTC, twelve general-purpose 16-bit timers including two PWM timers for motor control, two general-purpose 32-bit timers. A true random number generator (RNG).Figure 22 below shows how the discovery F4 board.[82]

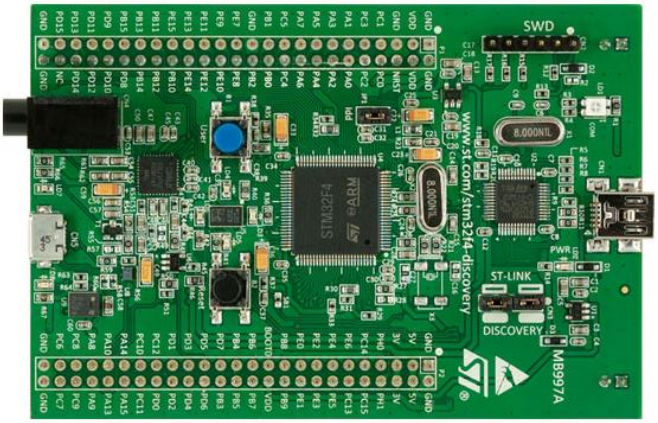

Figure 22. STM32F4 discovery board

Meade's LX90 telescope

The LX 90 shown in figure 23 below is an integral part of the receiver. This telescope features Meade's advanced coma free technology for high image clarity and a 12inch diameter, f/10 ACF optical system (focal length 3048mm) and UHTC for maximum image brightness and contrast. Electronics include the advanced Meade Audio-Star computer system with over 30,000 object library, multiple guided tours, High Precision Pointing capability, and Meade Smart Drive with Permanent Periodic Error Correction.[83]Precision star alignment by the LX90 is done near effortlessly with an incorporated 16 channel genuine Sony GPS receiver.[83]

Figure 23. The LX90 telescope

4.2.3 Software

The hardware listed in section 4.2.1 is useless without the software to control it. Different types of software are used in the simulation of the behavior or the receiver and just in the construction of the circuit such as:

- KiCAD
- LTSpice
- C programming language
- Stellarium

- Orbitron

Receiver schematic using KiCAD

The schematic and PCB were drawn and designed using KiCAD software. Figure 28 in appendix 2 shows the receiver schematic design circuit.

This receiver is made of 2 amplification stages and integrator to cancel out the SiMP's dark current.

Receiver PCB

Figure 24 below shows the designed receiver PCB.

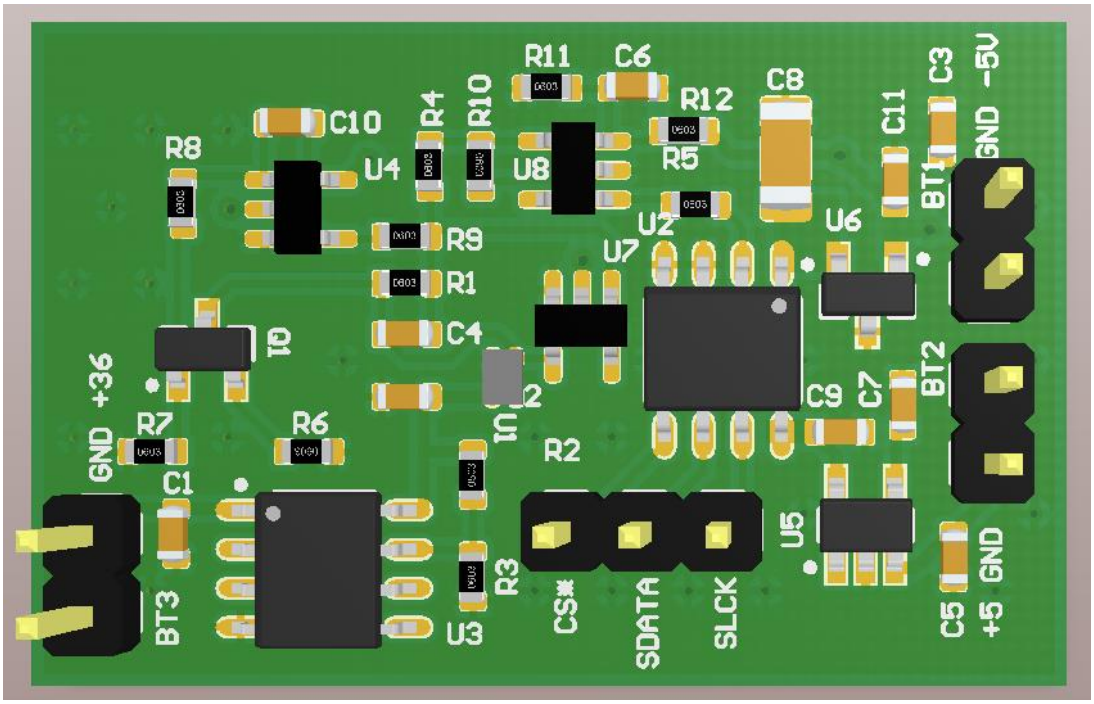

Figure 24. receiver PCB

Simulation results from LTSpice

This software was used to verify the receiver section of this project. It's where all the simulations of the amplifier were performed. The amplifier output is plotted in Figure 25 below. The integrator represented as V(n001) start working canceling out the excess current and control the first stage output. The integrator settles at approximately 20ms and the circuits functions normally. V(n006) is the out voltage of the integrator. V(output) is the amplifier output. The initial -5 to 5V is the switch transition period.

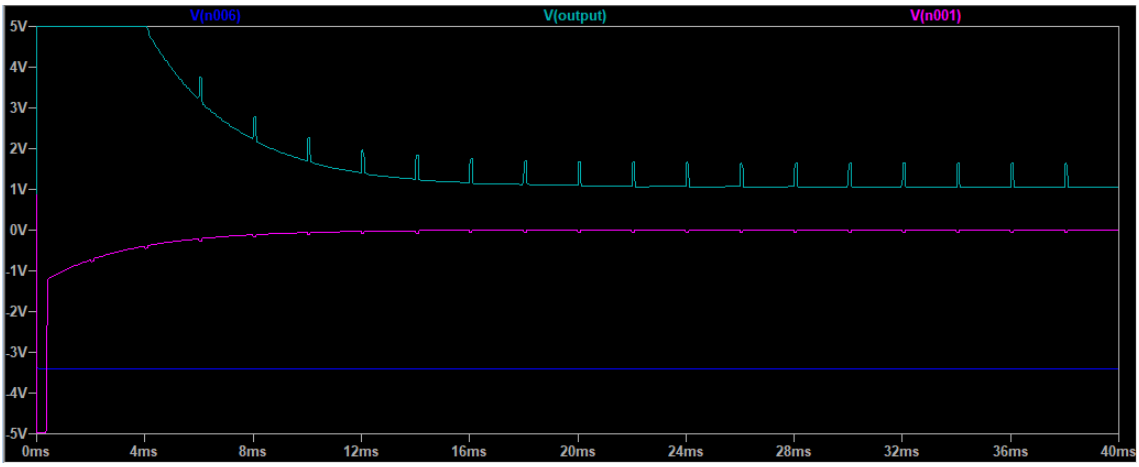

Figure 25. Amplifier performance

Space object movement Analysis and Tracking Software

This part of the software is an integral part of the receiver. The sky is vast and filled with all kinds of objects such as satellites, planets, nebulae; it's crucial that I can locate and track the satellite in space and this is where these software packs come in.

Stellarium

This is a free open source software for computers. It shows a realistic sky in 3D, just like what you see with the naked eye, binoculars or a telescope.[84] figure 26 below shows a screenshot from the program.

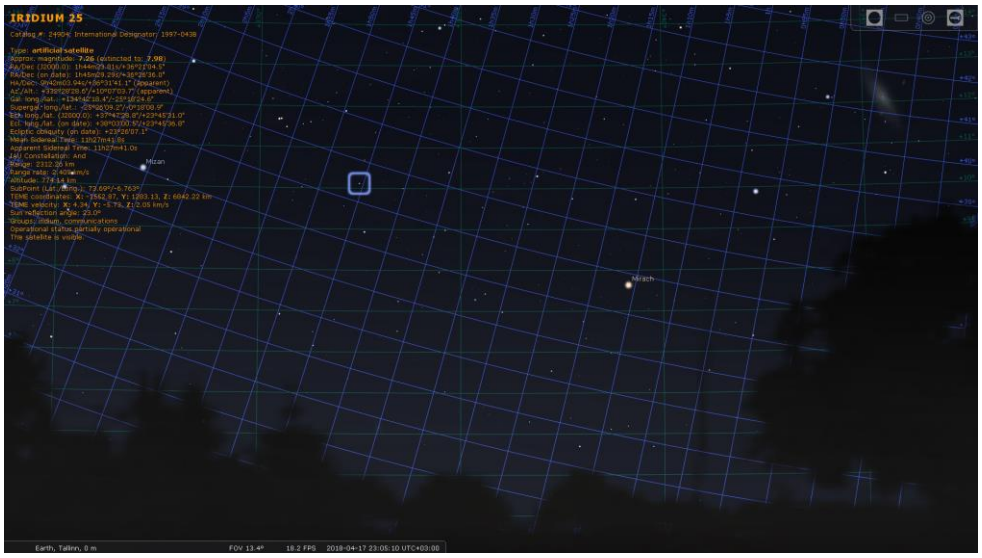

Figure 26. Screenshot of Stellarium tracking a satellite in orbit

Stellarium features

Stellarium has the capability to interface with and control the LX90 telescope [84]. Using the path coordinate data got from orbitron, a script can be created and the telescope will automatically track the satellite and position the receiver towards the signal source point.

Orbitron

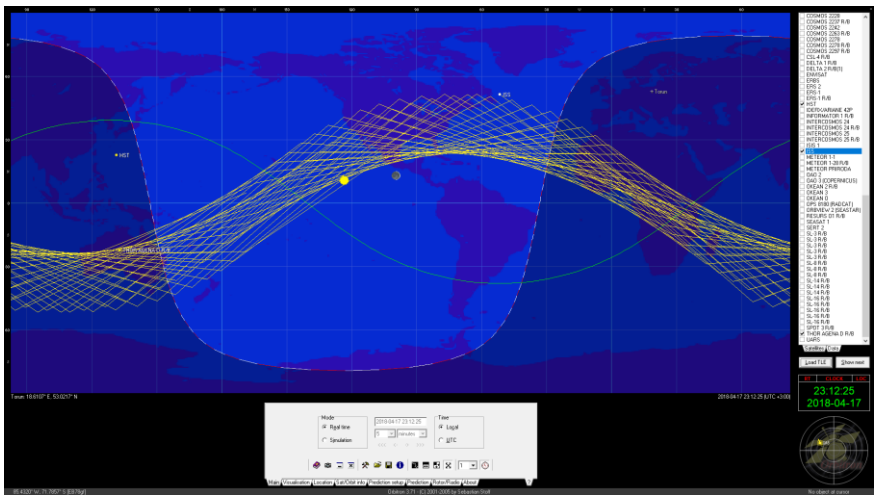

Figure 27. Screenshot of Orbitron tracking the ISS in orbit

Just like Stellarium, Orbitron performs object tracking in space just as seen in figure 27 above. In this thesis, however, Orbitron will be used to generate scripts containing coordinates that contain tracking data for objects in space. The data generated will be used to map and track the satellite path. Below in table 10 is a sample of how the generated data looks like.

Table 10. below shows some data extract from orbitron with coordinate predictions.

Satellite passes / Orbitron 3.71 / www.stoff.pl

Location : Torun (18.6107° E, 53.0217° N)

Time zone : UTC +3:00

Search period: 2018-04-19 10:39:14 - 3 days

2018-04-22 10:39:14

Conditions : Maximum sun elevation = -5 deg

Minimum sat elevation = 10 deg

Illumination required

Time	Satellite	Azm	Elv	Mag	Range	S.Azm	S.Elv
2018-04-19 21:23:07	ISS	314.5	10.9	16.9	578308	296.5	-5.1

2018-04-19 21:23:43	ISS	230.0	72.5	14.3574212	296.6 -5.2
2018-04-19 21:24:20	ISS	141.7	10.2	13.6580131	296.8 -5.2
2018-04-19 21:25:55	ISS	314.6	11.7	16.9578227	297.1 -5.5
2018-04-19 21:26:31	ISS	227.7	72.2	14.3574242	297.2 -5.5
2018-04-19 21:27:07	ISS	142.6	11.4	13.6579993	297.3 -5.6
2018-04-19 21:28:42	ISS	315.5	10.4	16.9578367	297.7 -5.8
2018-04-19 21:29:18	ISS	232.5	71.8	14.3574240	297.8 -5.9
2018-04-19 21:29:55	ISS	142.9	10.6	13.6580090	297.9 -6.0
2018-04-19 21:31:30	ISS	315.6	11.2	16.9578286	298.2 -6.2
2018-04-19 21:32:06	ISS	230.2	71.5	14.3574270	298.4 -6.3
2018-04-19 21:32:42	ISS	143.9	11.8	13.6579953	298.5 -6.4

The data generated by Orbitron will later be modified, and the coordinates will be coded into a different script that will be fed to the LX90 through Stellarium for semi-automated tracking.

5 Summary

The optical path was analyzed and path attenuation was calculated, link budget was calculated, the receiver gain was calculated, received power of -116.11 dBm on the ground was calculated and knowing the received power, an amplifier was designed and simulated with an SNR of 19dB and a BER in the 10^{-5} range. A receiver schematic and PCB were designed.

5.1 Future works

To improve the signal quality and link reliability, there is need to advance the research in the transmitter design by using stronger laser components, incorporate some optics after the laser in the transmitter part to control the divergence angle, and find a smoother and effective way to actively track the satellite in space and point the receiver where a concentration of the incident light falls. More time is also need to do a deeper study of space and atmospheric conditions and their effect on the signal. Data collection from a different point and sensor fusion is another, techniques to identify correlated photons by using a series of single photon sensitive sensors could be used. This doesn't eliminate the noise, instead, many samples are taken and used to create a distribution plot. As more values are added, a pattern can be formed. This mainly should be comprised of the photons correlated with the Tx. The sample collection can be aided with the use of a sample and hold system such as TI's LF 398 circuit. This technique is used in LIDAR systems as well. This way, this system can yield a better positive result. There are several prospects for future works.

5.2 Conclusion

The receiver was calculated and designed with an output of 1 Volt which is sufficient to drive the Analog to digital converter. An SNR of 19dB with a BER in the range of 10^{-5} allows receiving at 10kbps. The receiver design was the primary objective of this work and it was designed and simulated with positive results. This fulfils the requirements of this work.

References

[1] R. Garner, “Historic Demonstration Proves Laser Communication Possible,” 2015.

[2] J. Harbaugh, “Deep Space Optical Communications (DSOC),” 2017.

[3] Annamarie Nyirady, “NASA Awards PathFinder Digital Free Space Optics Contract - Via Satellite -,” 2019. [Online]. Available: https://www.satellitetoday.com/government-military/2019/04/25/nasa-awards-pathfinder-digital-free-space-optics-contract/. [Accessed: 09-May-2019].

[4] J. Feldmann, N. Youngblood, C. D. Wright, H. Bhaskaran, and W. H. P. Pernice, “All-optical spiking neurosynaptic networks with self-learning capabilities,” *Nature*, vol. 569, no. 7755, pp. 208–214, May 2019.

[5] L. Caspani *et al.*, “Integrated sources of photon quantum states based on nonlinear optics,” *Light Sci. Appl.*, vol. 6, no. 11, p. e17100, Nov. 2017.

[6] A. Aspuru-Guzik and P. Walther, “Photonic quantum simulators,” *Nat. Phys.*, vol. 8, no. 4, pp. 285–291, Apr. 2012.

[7] M. Zhang *et al.*, “Generation of multiphoton quantum states on silicon,” *Light Sci. Appl.*, vol. 8, no. 1, p. 41, Dec. 2019.

[8] C. Agnesi, M. Avesani, A. Stanco, P. Villoresi, and G. Vallone, “All-fiber self-compensating polarization encoder for quantum key distribution,” *Opt. Lett.*, vol. 44, no. 10, p. 2398, May 2019.

[9] J. A. Laurel Mackey, Jon Trump, Amy Valdez, “Global Free Space Optics (FSO) Communication Market Upcoming Trends, Growth Drivers, Opportunities and Challenges 2025 – Market Talk News.” [Online]. Available: https://markettalknews.com/global-free-space-optics-fso-communication-market-upcoming-trends-growth-drivers-opportunities-and-challenges-2025/. [Accessed: 09-May-2019].

[10] B. Demarr and S. De Janasz, “Advanced Electronic Communications Systems,”

p. 616, 2014.

[11] T. Greicius, “Psyche Overview,” 2017.

[12] “News | Deep Space Communications via Faraway Photons.” [Online]. Available: https://www.jpl.nasa.gov/news/news.php?feature=6967. [Accessed: 28-Mar-2018].

[13] “Golbriak Space.” [Online]. Available: https://golbriak.space/. [Accessed: 02-May-2018].

[14] “Google Lunar XPRIZE Home Page.” [Online]. Available: https://lunar.xprize.org/. [Accessed: 02-May-2018].

[15] “SpaceX.” [Online]. Available: http://www.spacex.com/. [Accessed: 02-May-2018].

[16] R. N. Vyvyan, *Marconi and wireless*. EP Pub, 1974.

[17] R. Vyvyan, *Wireless over thirty years*. Ann Arbor Mich.: University Microfilms International, 1983.

[18] R. A. Alsemmeari, S. T. Bakhsh, and H. Alsemmeari, “Free Space Optics Vs Radio Frequency Wireless Communication,” *I.J. Inf. Technol. Comput. Sci. Inf. Technol. Comput. Sci.*, vol. 9, no. 9, pp. 1–8, 2016.

[19] J. M. Kahn, J. R. Barry, and M. D. Audeh, “Free-space Infrared Communication For Wireless Local-area Networks,” in *LEOS ’92 Conference Proceedings*, pp. 236–237.

[20] Jones Newell, “First ‘Radio’ Built by San Diego Resident Partner of Inventor of Telephone: Keeps Notebook of Experiences With Bell,” 1937.

[21] D. L. HUTT, K. J. SNELL, and P. A. BÉLANGER, “Alexander Graham Bell’s PHOTOPHONE,” *Opt. Photonics News*, vol. 4, no. 6, p. 20, Jun. 1993.

[22] I. K. Son and S. Mao, “A survey of free space optical networks,” *Digit. Commun. Networks*, vol. 3, no. 2, pp. 67–77, May 2017.

[23] Nasa, “Deep Space Optical Communications (DSOC) | Space Technology: Game Changing Development.” [Online]. Available: https://gameon.nasa.gov/projects-2/archived-projects-2/deep-space-optical-communications-dsoc/. [Accessed: 20-Apr-2018].

[24] “Capturing a Whisper from a Billion Kilometers.”

[25] E. Ciaramella *et al.*, “1.28 terabit/s (32x40 Gbit/s) wdm transmission system for free space optical communications,” *IEEE J. Sel. Areas Commun.*, vol. 27, no. 9, pp. 1639–1645, Dec. 2009.

[26] Doug Massier, “DLR Researchers Set World Record in Free-space Optical Communications – Parabolic Arc.” [Online]. Available: http://www.parabolicarc.com/2016/11/05/dlr-researchers-set-world-record-freespace-optical-communications/. [Accessed: 20-Apr-2018].

[27] G. Diviney, “No Title,” *An Introd. to Short-Range Wirel. Data Commun.*

[28] X. Wang and S. Mao, “A SURVEY OF LTE WI-FI COEXISTENCE IN UNLICENSED BANDS,” *GetMobile*, vol. 20, no. 3, 2016.

[29] C. C. Davis, I. I. Smolyaninov, and S. D. Milner, “Flexible optical wireless links and networks,” *IEEE Commun. Mag.*, vol. 41, no. 3, pp. 51–57, Mar. 2003.

[30] A. Mahdy and J. S. Deogun, “Wireless optical communications: a survey,” in *2004 IEEE Wireless Communications and Networking Conference (IEEE Cat. No.04TH8733)*, pp. 2399–2404.

[31] S. Vangala and H. Pishro-Nik, “Optimal Hybrid RF-Wireless Optical Communication for Maximum Efficiency and Reliability,” in *2007 41st Annual Conference on Information Sciences and Systems*, 2007, pp. 684–689.

[32] K.-D. Langer and J. Grubor, “Recent Developments in Optical Wireless Communications using Infrared and Visible Light,” in *2007 9th International Conference on Transparent Optical Networks*, 2007, pp. 146–151.

[33] V. W. S. Chan, “Free-Space Optical Communications,” *J. Light. Technol.*, vol. 24, no. 12, pp. 4750–4762, Dec. 2006.

[34] Xiaoming Zhu and J. M. Kahn, “Free-space optical communication through atmospheric turbulence channels,” *IEEE Trans. Commun.*, vol. 50, no. 8, pp. 1293–1300, Aug. 2002.

[35] M. Abtahi, P. Lemieux, W. Mathlouthi, and L. A. Rusch, “Suppression of Turbulence-Induced Scintillation in Free-Space Optical Communication Systems Using Saturated Optical Amplifiers,” *J. Light. Technol.*, vol. 24, no. 12, pp. 4966–4973, Dec. 2006.

[36] V. W. S. Chan, “Free-Space Optical Communications,” *J. Light. Technol.*, vol. 24, no. 12, pp. 4750–4762, Dec. 2006.

[37] D. J. T. Heatley, D. R. Wisely, I. Neild, and P. Cochrane, “Optical wireless: the story so far,” *IEEE Commun. Mag.*, vol. 36, no. 12, pp. 72–74, 79–82, 1998.

[38] C. Y. H. Larry C. Andrews, Ronald L. Phillips, *Laser Beam Scintillation with Applications - Larry C. Andrews, Ronald L. Phillips, Cynthia Y. Hopen - Google Books*. SPIE PRESS, 2001.

[39] J. Juarez, A. Dwivedi, A. Hammons, S. Jones, V. Weerackody, and R. Nichols, “Free-Space Optical Communications for Next-generation Military Networks,” *IEEE Commun. Mag.*, vol. 44, no. 11, pp. 46–51, Nov. 2006.

[40] B. Epple and H. Henniger, “Discussion on design aspects for free-space optical communication terminals,” *IEEE Commun. Mag.*, vol. 45, no. 10, pp. 62–69, Oct. 2007.

[41] G. Baister and P. V. Gatenby, “Pointing, acquisition and tracking for optical space communications,” *Electron. Commun. Eng. J.*, vol. 6, no. 6, pp. 271–280, Dec. 1994.

[42] F. Liu, U. Vishkin, and S. Milner, “Bootstrapping free-space optical networks,” *IEEE J. Sel. Areas Commun.*, vol. 24, no. 12, pp. 13–22, Dec. 2006.

[43] S. Navidpour, M. Uysal, and M. Kavehrad, “BER Performance of Free-Space Optical Transmission with Spatial Diversity,” *IEEE Trans. Wirel. Commun.*, vol. 6, no. 8, pp. 2813–2819, Aug. 2007.

[44] E. J. Lee and V. W. S. Chan, “Part 1: Optical Communication Over the Clear Turbulent Atmospheric Channel Using Diversity,” *IEEE J. Sel. Areas Commun.*, vol. 22, no. 9, pp. 1896–1906, Nov. 2004.

[45] H. Izadpanah, T. ElBatt, V. Kukshya, F. Dolezal, and B. K. Ryu, “High-availability free space optical and RF hybrid wireless networks,” *IEEE Wirel. Commun.*, vol. 10, no. 2, pp. 45–53, Apr. 2003.

[46] A. Desai and S. Milner, “Autonomous reconfiguration in free-space optical sensor networks,” *IEEE J. Sel. Areas Commun.*, vol. 23, no. 8, pp. 1556–1563, Aug. 2005.

[47] M. Kavehrad and S. Jivkova, “Indoor broadband optical wireless communications: optical subsystems designs and their impact on channel characteristics,” *IEEE Wirel. Commun.*, vol. 10, no. 2, pp. 30–35, Apr. 2003.

[48] M. N. Smadi, S. C. Ghosh, A. A. Farid, T. D. Todd, and S. Hranilovic, “Free-Space Optical Gateway Placement in Hybrid Wireless Mesh Networks,” *J. Light. Technol.*, vol. 27, no. 14, pp. 2688–2697, Jul. 2009.

[49] T. Nakai, K. Takazawa, and H. Ando, “INFORMATION RECORDING MEDIUM, INFORMATION RECORDING/PLAYBACK APPARATUS, INSPECTION METHOD OF INFORMATION RECORDING MEDIUM, AND INSPECTION APPARATUS OF INFORMATION RECORDING MEDIUM,” Jan. 2008.

[50] M. Zuliyana, M. S. Anuar, S. A. Aljunid, A. K. Rahman, C. B. M Rashidi, and M. S. A Bakar, “PERFORMANCE ANALYSIS OF FSO WITH HAZE ATTENUATION CONSEQUENCE ACCLIMATIZE IN TROPICAL RAINFOREST ENVIRONMENT,” vol. 10, no. 3, 2015.

[51] J. C. R. Arun K. Majumdar, *Free-Space Laser Communications - Arun K. Majumdar | Absorption Spectroscopy | Electromagnetic Spectrum*. Springer.

[52] A. G. Al-Ghamdi and J. M. H. Elmirghani, “Analysis of Diffuse Optical Wireless Channels Employing Spot-Diffusing Techniques, Diversity Receivers, and Combining Schemes,” *IEEE Trans. Commun.*, vol. 52, no. 10, pp. 1622–1631,

Oct. 2004.

[53] C. Chen, H. Yang, J. Fan, Y. Ding, and C. Han, “Field-of-View Optimization of FSO Receiver Using Real-coded Genetic Algorithm,” in *2010 International Conference on Artificial Intelligence and Computational Intelligence*, 2010, pp. 459–462.

[54] E. Clements *et al.*, “Nanosatellite optical downlink experiment: design, simulation, and prototyping,” *Opt. Eng.*, vol. 55, no. 11, p. 111610, Sep. 2016.

[55] Renesas, “ISL29023 Datasheet,” 2014.

[56] Renesas, “ISL29033 Datasheet,” 2016.

[57] “Human beings obtain more.”

[58] “RB−Series SiPM Sensors.”

[59] “PHOTOMULTIPLIER TUBES AND ASSEMBLIES FOR SCINTILLATION COUNTING & HIGH ENERGY PHYSICS.”

[60] S. Piatek, “Silicon Photomultiplier.”

[61] “Encyclopedia of Laser Physics and Technology - photodiodes, photodetectors, p-i-n, InGaAs, silicon, germanium, PIN, bandwidth, linearity, current amplifier.” .

[62] R. Paschotta, “Encyclopedia of Laser Physics and Technology - p-i-n photodiodes, PIN photodiode.” [Online]. Available: https://www.rp-photonics.com/p_i_n_photodiodes.html. [Accessed: 18-Apr-2018].

[63] R. Paschotta, *Encyclopedia of laser physics and technology*. Wiley-VCH, 2008.

[64] H. Dautet *et al.*, “Photon counting techniques with silicon avalanche photodiodes,” 1993.

[65] L. Pancheri, G.-F. Dalla Betta, and D. Stoppa, “CMOS avalanche photodiodes for sub-ns time-resolved images,” *SPIE Newsroom*, Jun. 2014.

[66] B. F. Aull *et al.*, “Large-Format Geiger-Mode Avalanche Photodiode Arrays and

Readout Circuits," *IEEE J. Sel. Top. QUANTUM Electron.*, vol. 24, no. 2, p. 3800510.

[67] P. Kostoulas and S. Applications Engineer, "Geiger-Mode Sensing Technology Geiger-mode LiDAR-The Dawn of Digital Mapping Geiger-Mode Sensing Technology 3 Geiger-mode Sensing Technology."

[68] ffyvgq, "AND9770 - Introduction to the Silicon Photomultiplier (SiPM)."

[69] W.-C. Wang, "Optical Detectors."

[70] Panasonic, "LNCT22PK01WW," 2018.

[71] "CHAPTER-5 Estimation of FSO Link Availability Using Climatic Data 5.1 Introduction."

[72] Robert Keim, "Understanding and Implementing Charge Amplifiers for Piezoelectric Sensor Systems." [Online]. Available: https://www.allaboutcircuits.com/technical-articles/understanding-and-implementing-charge-amplifiers-for-piezoelectric-sensor-s/. [Accessed: 03-May-2019].

[73] "Characteristics and use of Charge amplifier SOLID STATE DIVISION."

[74] X. Ramus, "Transimpedance Considerations for High-Speed Amplifiers," 2009.

[75] C. Kitchin and L. Counts, "A DESIGNER'S GUIDE TO INSTRUMENTATION AMPLIFIERS 3 RD Edition."

[76] L. Technology Corporation, "LTC6240/LTC6241/LTC6242 - Single/Dual/Quad 18MHz, Low Noise, Rail-to-Rail Output, CMOS Op Amps."

[77] Q. Chen, W. Zheng, T. Zhang, W. Cui, and Z. Cui, "A power analysis model for outdoor long-distance visible light communication," in *2017 Ninth International Conference on Ubiquitous and Future Networks (ICUFN)*, 2017, pp. 131–136.

[78] T. Y. Elganimi, "Studying the BER performance, power- and bandwidth-efficiency for FSO communication systems under various modulation schemes," in *2013 IEEE Jordan Conference on Applied Electrical Engineering and*

Computing Technologies (AEECT), 2013, pp. 1–6.

[79] "UV VIS NIR optical filters | Absorption interference filters | Interference bandpass filters." [Online]. Available: https://www.knightoptical.com/stock/optical-components/uvvisnir-optics/filters/. [Accessed: 11-Dec-2018].

[80] "Photodetectors for LiDAR Hamamatsu offers solution for LiDAR applications with various devices APD Photosensor with front-end IC PIN photodiode MPPC (multi-pixel photo counter)," 2018.

[81] A. Devices, "AD7450 Differential Input, 1 MSPS 12-Bit ADC."

[82] STMicroelectronics, "STM32F407VG - High-performance foundation line, ARM Cortex-M4 core with DSP and FPU, 1 Mbyte Flash, 168 MHz CPU, ART Accelerator, Ethernet, FSMC - STMicroelectronics," 2018. [Online]. Available: http://www.st.com/en/microcontrollers/stm32f407vg.html. [Accessed: 17-Apr-2018].

[83] "LX90-ACF 12" f/10 (No Tripod) Telescopes, Solar Telescopes, Binoculars, Spotting Scopes." [Online]. Available: https://www.meade.com/lx90-acf-12-f-10-no-tripod.html#product_tabs_additional. [Accessed: 16-Apr-2018].

[84] Stellarium, "Stellarium Astronomy Software." [Online]. Available: http://stellarium.org/. [Accessed: 18-Apr-2018].

Appendix 1 – ADC Snippet in Interleaved mode

```
/**
 * @brief Get the average of N-X ADC samples
 * @param Numbre of ADC samples to be averaged
 * @param Numbre of ADC samples to be averaged
 * @retval The average value
 */
uint16_t ADC_GetSampleAvgNDeleteX(uint8_t N , uint8_t X)
{
 uint32_t avg_sample =0x00;
 uint16_t adc_sample[8]={0,0,0,0,0,0,0,0};
 uint8_t index=0x00;
 for (index=0x00; index<N; index++)
  {
    /* ADC start conv */
    ADC_SoftwareStartConv(ADC1);
    /* Wait end of conversion */
    while(ADC_GetFlagStatus(ADC1,ADC_FLAG_EOC) == RESET);
    /* Store ADC samples */
    adc_sample[index] = ADC_GetConversionValue(ADC1);
```

```
  }
 /* Sort the N-X ADC samples */
 Sort_tab(adc_sample,N);
 /* Add the N ADC samples */
 for (index=X/2; index<N-X/2; index++)
 {
   avg_sample += adc_sample[index];
 }
   /* Compute the average of N-X ADC sample */
   avg_sample /= N-X;
   /* Return average value */
 return avg_sample;
}
  /*
    * @brief Sort the N ADC samples
    * @param ADC samples to be sorted
    * @param Numbre of ADC samples to be sorted
    * @retval None
    */
void Sort_tab(uint16_t tab[], uint8_t lenght)
{
```

```
  uint8_t l=0x00, exchange =0x01;
  uint16_t tmp=0x00;
  /* Sort tab */
  while(exchange==1)
  {
    exchange=0;
    for(l=0; l<lenght-1; l++)
  {
    if( tab[l] > tab[l+1] )
  {
    tmp = tab[l];
    tab[l] = tab[l+1];
    tab[l+1] = tmp;
    exchange=1;
  }
    }
  }
}
```

Appendix 2 - More of the schematics

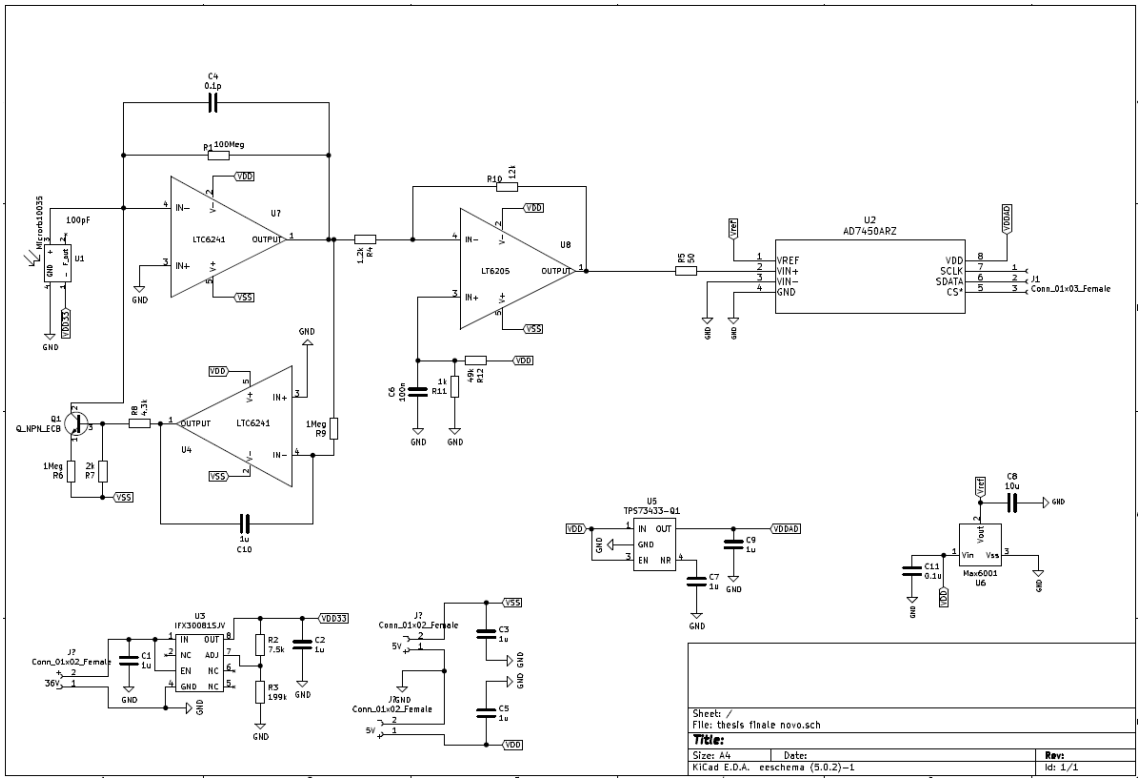

Figure 28. STM32 schematic

Appendix 3 – ADC initialization in C language

```
/* ADC1 init function */
static void MX_ADC1_Init(void)
{

  ADC_ChannelConfTypeDef sConfig;

    /**Configure Clock, Resolution, Data Alignment and
number of conversion
    */
  hadc1.Instance = ADC1;
  hadc1.Init.ClockPrescaler = ADC_CLOCK_SYNC_PCLK_DIV4;
  hadc1.Init.Resolution = ADC_RESOLUTION_12B;
  hadc1.Init.ScanConvMode = DISABLE;
  hadc1.Init.ContinuousConvMode = DISABLE;
  hadc1.Init.DiscontinuousConvMode = DISABLE;
  hadc1.Init.ExternalTrigConvEdge                          =
ADC_EXTERNALTRIGCONVEDGE_NONE;
  hadc1.Init.ExternalTrigConv = ADC_SOFTWARE_START;
  hadc1.Init.DataAlign = ADC_DATAALIGN_RIGHT;
  hadc1.Init.NbrOfConversion = 1;
  hadc1.Init.DMAContinuousRequests = DISABLE;
  hadc1.Init.EOCSelection = ADC_EOC_SINGLE_CONV;
  if (HAL_ADC_Init(&hadc1) != HAL_OK)
  {
    _Error_Handler(__FILE__, __LINE__);
  }

    /**Configure for the selected ADC regular channel its
corresponding rank in the sequencer and its sample time.
    */
  sConfig.Channel = ADC_CHANNEL_1;
  sConfig.Rank = 1;
  sConfig.SamplingTime = ADC_SAMPLETIME_3CYCLES;
  if (HAL_ADC_ConfigChannel(&hadc1, &sConfig) != HAL_OK)
  {
    _Error_Handler(__FILE__, __LINE__);
  }

}
```